AGU PUBLICATIONS

Geochemistry, Geophysics, Geosystems

RESEARCH ARTICLE
10.1002/2017GC006975

Special Section:
Carbon Degassing Through Volcanoes and Active Tectonic Regions

Spatially Variable CO_2 Degassing in the Main Ethiopian Rift: Implications for Magma Storage, Volatile Transport, and Rift-Related Emissions

Jonathan A. Hunt[1], Amdemichael Zafu[2], Tamsin A. Mather[1], David M. Pyle[1], and Peter H. Barry[1,3]

[1]Department of Earth Sciences, University of Oxford, Oxford, UK, [2]School of Earth Sciences, Addis Ababa University, Addis Ababa, Ethiopia, [3]California Water Science Center, USGS, San Diego, CA, USA

Key Points:
- New gas surveys show that diffuse CO_2 degassing in the Main Ethiopian Rift is highly variable, concentrated along faults in geothermal areas
- Locations of hot springs and fumaroles indicate numerous (~14–20) geothermal areas some distance from major volcanic edifices
- Extrapolation from our data suggests a total diffuse CO_2 flux from the Main Ethiopian Rift of 0.5–4.4 Mt yr^{-1} (whole Eastern Rift: 4–33 Mt yr^{-1})

Supporting Information:
- Supporting Information S1
- Table S1
- Table S2

Correspondence to:
J. Hunt,
jonathan.hunt@earth.ox.ac.uk

Citation:
Hunt, J. A., Zafu, A., Mather, T. A., Pyle, D. M., & Barry, P. H. (2017). Spatially variable CO_2 degassing in the Main Ethiopian Rift: Implications for magma storage, volatile transport, and rift-related emissions. *Geochemistry, Geophysics, Geosystems*, *18*, 3714–3737. https://doi.org/10.1002/2017GC006975

Received 14 APR 2017
Accepted 21 SEP 2017
Accepted article online 28 SEP 2017
Published online 30 OCT 2017

Abstract Deep carbon emissions from historically inactive volcanoes, hydrothermal, and tectonic structures are among the greatest unknowns in the long-term (~Myr) carbon cycle. Recent estimates of diffuse CO_2 flux from the Eastern Rift of the East African Rift System (EARS) suggest this could equal emissions from the entire mid-ocean ridge system. We report new CO_2 surveys from the Main Ethiopian Rift (MER, northernmost EARS), and reassess the rift-related CO_2 flux. Since degassing in the MER is concentrated in discrete areas of volcanic and off-edifice activity, characterization of such areas is important for extrapolation to a rift-scale budget. Locations of hot springs and fumaroles along the rift show numerous geothermal areas away from volcanic edifices. With these new data, we estimate total CO_2 emissions from the central and northern MER as 0.52–4.36 Mt yr^{-1}. Our extrapolated flux from the Eastern Rift is 3.9–32.7 Mt yr^{-1} CO_2, overlapping with lower end of the range presented in recent estimates. By scaling, we suggest that 6–18 Mt yr^{-1} CO_2 flux can be accounted for by magmatic extension, which implies an important role for volatile-enriched lithosphere, crustal assimilation, and/or additional magmatic intrusion to account for the upper range of flux estimates. Our results also have implications for the nature of volcanism in the MER. Many geothermal areas are found >10 km from the nearest volcanic center, suggesting ongoing hazards associated with regional volcanism.

Plain Language Summary The amount of carbon dioxide seeping out of the Earth's surface is poorly understood. Magma carries dissolved carbon dioxide from the deep earth toward the surface, where it is released and travels along fractures in the crust. This study attempts to quantify this phenomenon in central Ethiopia, where a continental rift is splitting one tectonic plate in two. In Kenya and Tanzania, a similar study suggested that the flow of carbon dioxide through the East African Rift was much larger than previously thought. We undertook new surveys and found that it varies greatly, which makes estimating a total flow through the rift very difficult. The distribution of hot springs and volcanic vents provides clues concerning where heat and carbon dioxide come to the surface—by compiling the locations of these features we were able to extrapolate from our surveys for a new estimate. Our results suggest that the East African Rift releases less carbon dioxide than was thought from Kenya and Tanzania, but still a substantial amount. If the rift does emit as much carbon dioxide as suggested, either more carbon is below the crust in East Africa than we thought or more magma is involved.

1. Introduction

Volcanic systems make a substantial contribution to the long-term release of volatile species from the mantle. There is significant interest in understanding the nature of the "deep carbon" cycle, particularly that associated with the fluxes of magma out of the mantle (Dasgupta, 2013; Kelemen & Manning, 2015); on long time scales (~Myr), carbon fluxes from the mantle have a major influence on the global carbon cycle and are an important mechanism in natural climate variability (Dasgupta, 2013). However, there remain significant gaps in our knowledge of the deep carbon fluxes associated with magmatism, especially from magmas that end up stored within the lithosphere, rather than being erupted. In recent reviews of deep carbon emissions, Burton et al. (2013) and Mörner and Etiope (2002) highlight the dominance of long-term continuous, passive CO_2 degassing over that from short-lived eruptions. It is clearly important to quantify passive emissions if we are to better understand the global carbon cycle.

There is growing recognition that diffuse degassing represents a significant proportion of the total passive CO_2 flux at a number of volcanoes, e.g., Etna (Allard et al., 1997; D'Alessandro et al., 1997), Pantelleria (Favara et al., 2001), Campi Flegrei (Chiodini et al., 2001), and Long Valley Caldera (Lucic et al., 2015). This is in part due to the low solubility of CO_2 in magmas, which means that it can degas at great depths within the Earth's crust and percolate out over a wider area than shallower emissions. CO_2 emissions from historically inactive volcanoes, hydrothermal, and tectonic structures are a poorly constrained component of the global deep CO_2 budget (Burton et al., 2013).

Diffuse carbon degassing from volcanic fields is challenging to quantify given their large areal extent, heterogeneous nature, and complex fluid flow regimes. The few existing surveys focus on a small number of restless calderas in Italy and Yellowstone, which may not be representative of calderas worldwide (Chiodini et al., 1999, 2004, 2007, 2010; Chiodini & Frondini, 2001; Etiope et al., 1999; Giammanco et al., 2007; Italiano et al., 2000; Mörner & Etiope, 2002; Rogie et al., 2000; Werner & Brantley, 2003). Burton et al. (2013) provide an estimate of global emissions from historically inactive volcanoes, hydrothermal, and tectonic structures of >66 Mt yr^{-1} CO_2; the current estimate rises to >137 Mt yr^{-1} CO_2 when accounting for recent work on degassing from tectonic structures in East Africa (Lee et al., 2016). This estimate is largely derived from just four study areas (Central Italy, Chiodini et al., 2004; Taupo Volcanic Zone, Seward & Kerrick, 1996; Yellowstone, Werner & Brantley, 2003; and Kenya Rift Valley, Lee et al., 2016) and depends heavily on extrapolation from emissions associated with the Taupo Volcanic Zone to the entire Pacific Rim (44 Mt yr^{-1}; Seward & Kerrick, 1996). These estimates are compiled in Figure 1. The lack of representative surveys hinders our ability to determine an upper bound for global, deep degassing from tectonic structures, particularly given the occurrence of very high flux but spatially restricted areas (e.g., Mefite, Italy; Chiodini et al., 2010). It is likely that the contribution from Pacific Rim settings is larger than current estimates suggest, given the proportionately higher fluxes recorded in smaller regions.

Continental rifts may be an important contributor to deep, diffuse carbon fluxes. Elevated magmatic fluxes, and an abundance of faults and fractures along which CO_2 can migrate, provide both a source of carbon and mechanisms for release (Figure 2; Hutchison et al., 2015; Lee et al., 2016; Muirhead et al., 2016). Melts generated in continental rift settings may be alkaline with elevated CO_2 contents, whether due to an enriched and/or metasomatized source region, or conditions of partial of melting (e.g., Ferguson et al., 2013; Hudgins et al., 2015). CO_2 and other volatiles are carried into the lithosphere as the melt is intruded,

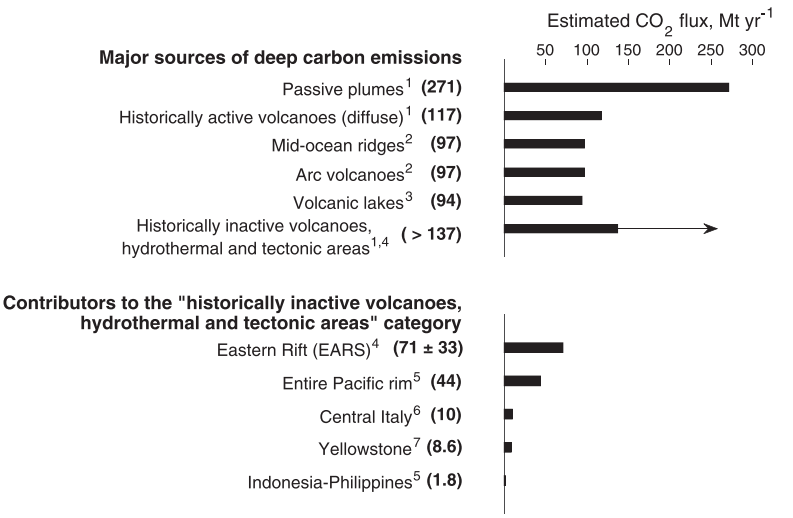

Figure 1. Deep CO_2 flux estimates compiled by Burton et al. (2013) and developed by Lee et al. (2016). (top) Major contributors to the deep carbon budget. The lack of observations of emissions from historically inactive volcanoes, hydrothermal, and tectonic areas prevents an estimate of an upper bound. (bottom) Major contributors from the "historically inactive volcanoes, hydrothermal and tectonic structures" group, including the East African Rift (Lee et al., 2016). The current EARS flux estimate exceeds early estimates for the entire Pacific Rim (18,000 km of arc volcanoes). References: [1]Burton et al. (2013), [2]Marty and Tolstikhin (1998), [3]Pérez et al. (2011), [4]Lee et al. (2016), [5]Seward and Kerrick (1996), [6]Chiodini et al. (2004), and [7]Werner and Brantley (2003).

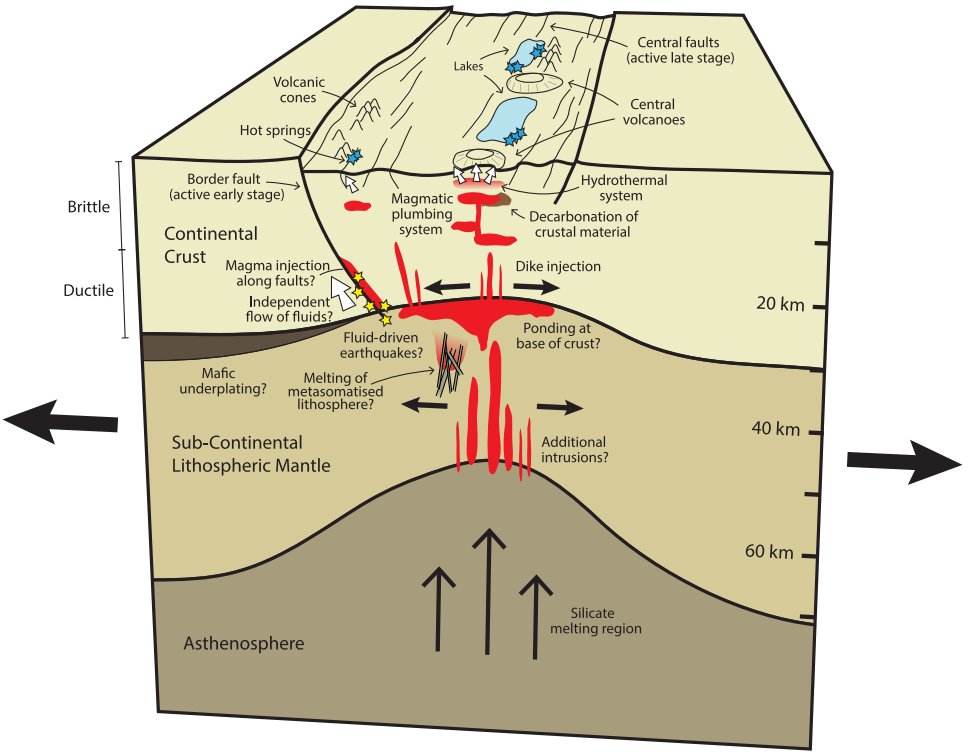

Figure 2. Paths for CO_2 degassing out of a continental rift. White arrows denote CO_2 fluid flow; blue stars, hot springs; and yellow stars denote deep earthquakes. CO_2 travels with the melt and independently along low permeability pathways.

enabling and accommodating extension. Intrusion and melting of metasomatized, volatile-enriched lithosphere may be an important process in rift development, transporting heat and fluids which weaken the surrounding material (Rooney et al., 2011, 2014, 2017). Magma may pool and underplate or intrude the crust (e.g., Plasman et al., 2017), and fluids may move independently to the surface if the permeability of the local rocks is low. Permeability decreases with pressure and increases in fault damage zones; CO_2 therefore flows freely in the fractured, shallow crust (Etiope & Martinelli, 2002; Faulkner et al., 2010). The extent to which large faults may facilitate CO_2 flow in the deep crust is unclear, although some deep earthquakes have been interpreted as fluid-driven (e.g., Albaric et al., 2014; Keir et al., 2009; Reyners et al., 2007). Magma may also intrude along these large faults, bringing CO_2 toward the surface (e.g., Italiano et al., 2000).

Continental rifts vary in maturity, from large, fault-bounded basins (e.g., North Tanzanian Divergence; Ebinger, 2005) to incipient seafloor spreading (e.g., Red Sea Rift; Keranen & Klemperer, 2008; Wright et al., 2006). Studying CO_2 emissions from continental rifts may help to constrain degassing from their potential successors, mid-ocean ridges (MORs), and refine estimates for modern-day and past geological CO_2 fluxes to the atmosphere. Quantifying the long-term carbon budget from the solid-earth is important for our understanding of long-term geological feedbacks, environmental change, and mass extinction events (e.g., Berner et al., 1983; Self et al., 2006; Wignall, 2001). The location and magnitude of degassing from continental rifts may also prove useful for identifying areas of magma storage, assessing the relative activity of volcanic systems (e.g., Evans et al., 2009) and investigating rift architecture with respect to fault activity (Muirhead et al., 2016). The extent to which CO_2-rich fluids flow through faults is a key area of research, with implications for trapping and sealing CO_2 for storage (e.g., Dockrill & Shipton, 2010). In extreme cases, CO_2 leakage from the subsurface may result in the accumulation of lethal concentrations, presenting a hazard to life (Chiodini et al., 2010; Hernández Perez et al., 2003; Smets et al., 2010).

The largest continental rift on Earth is the East African Rift System (EARS), which cuts through the African continent and separates the Nubian and Somali plates. The system is subdivided into a number of rifts, including the Main Ethiopian Rift (MER; from southern Afar to Lake Turkana) and the Kenya Rift Valley (KRV;

from Lake Turkana to the North Tanzanian Divergence). A recent diffuse CO_2 survey in the southernmost KRV found that faults in the Natron and Magadi basins were responsible for ~4 Mt yr^{-1} CO_2 release, implying that large carbon emissions may be associated with deep degassing from tectonic structures (Lee et al., 2016). The estimate of mantle-derived, diffuse soil flux from the Natron region (1.09–3.83 Mt yr^{-1}; Lee et al., 2016) is an order of magnitude higher than CO_2 flux estimates due to springs in the Natron region, based on carbon concentrations in fluids and discharge rates (0.022 Mt yr^{-1}; Barry et al., 2013; 0.23 Mt yr^{-1}; Lee et al., 2017). This result suggests a strong partitioning of CO_2 transport toward diffuse degassing rather than via fluid advection.

By scaling up their results, Lee et al. (2016) suggested that the diffuse CO_2 contribution from the Eastern Rift of the EARS (comprising the MER and KRV) could be as much as 38–104 Mt yr^{-1}, comparable to the entire MOR system (Figure 1). As acknowledged by the authors, more work is required to investigate whether these findings apply to the rift system as a whole, or whether the basins are themselves anomalous. The crust in the KRV is considered to be thicker and older than elsewhere in the rift, with accordingly more potential for reworking and assimilation of crustal carbon (Lee et al., 2017). Elevated CO_2 emissions have been recorded from the nearby carbonatite volcano of Oldoinyo Lengai (Koepenick et al., 1996; Oppenheimer et al., 2002). Although this style of volcanism may reflect unusually high concentrations of mantle carbon, the volatile composition of Oldoinyo Lengai is indistinguishable from mid-ocean ridge volatiles (Fischer et al., 2009). Consequently, high concentrations of carbon in Lengai lavas may be the result of immiscibility rather than compositional differences in the crust or mantle (e.g., Dawson et al., 1996).

The isotopic composition of the sampled CO_2 from the Magadi and Natron basins (–3.8 to $-11.7‰$) overlaps with the composition of both air (–8‰), and mantle sources (–3 to $-8‰$). Lee et al. (2016) interpret these data as requiring a significant mantle contribution, however an alternative interpretation of the isotope data would suggest an admixture between air-derived, biogenic, and mantle contributions and thus a potentially smaller mantle-derived CO_2 contribution. Extrapolation of the elevated CO_2 fluxes from the Magadi and Natron basins to the entire Eastern Rift suggests that the rift-scale deep carbon flux may be significantly higher than previously thought (Lee et al., 2016). Their conclusions imply an elevated flux of mantle-derived CO_2 per unit length of rift compared to MORs (3,000 km versus 60,000 km). This hypothesis has important implications for both the magmatic flux to the rift, and the mantle carbon contents required to sustain degassing.

Surveys elsewhere in the EARS suggest that the nature of carbon degassing varies substantially between localities and between volcanoes, and that point source fluxes may vary widely. For example, the CO_2 flux from individual rift volcanoes varies by more than 2 orders of magnitude (Aluto, 90–180 kt yr^{-1}; Hutchison et al., 2015; Longonot, 0.1 kt yr^{-1}; Robertson et al., 2016). The challenge in a rift system that exhibits diverse degassing styles and fluxes across a range of length scales is to integrate the available data to estimate the deep carbon flux to the surface.

Here we report new observations from field surveys, compile areas of geothermal manifestations and characterize the distribution of areas of high carbon flux in the Main Ethiopian Rift (MER). We develop an alternative estimate for rift-scale, diffuse CO_2 flux, based on localized areas of strong degassing.

1.1. Regional Context

The MER started to develop in the Oligocene with the emplacement of continental flood basalts (Wolde-Gabriel et al., 1990) and progressed from initial mechanical extension on large border faults to focused strain accommodation within central magmatic segments (Abebe et al., 2007; Ebinger & Casey, 2001). Magmatic intrusion promotes extension in continental rifts, weakening the lithosphere (e.g., Buck, 2004). As rifting progresses, the concentration of strain to the center of the rift is enabled by the location of magmatism, with magmatic intrusion accommodating an increasing proportion of extension (e.g., Keir et al., 2006; Rooney et al., 2011). This leads to colocation of magmatism and faulting on the surface and associated gas release (Muirhead et al., 2016)—magmatism supports extension and faulting which is assisted by volatile release, and the increased faulting enables an increase in volatile transport.

Surface magmatism in the MER takes two distinct forms: large silicic volcanoes and distributed mafic cones (e.g., Abebe et al., 2007). In the central MER, two parallel zones with high fault and cone density run approximately NNE-SSW; the Silti-Debre Zeyit Fault Zone (SDFZ) on the western margin of the rift has a lower fault

density than the Wonji Fault Belt (WFB) on the eastern margin. In the more mature northern MER, the WFB acts as an axial spreading center and the SDFZ is absent (Agostini et al., 2011; WoldeGabriel et al., 1990).

The present-day locations of magma storage within the MER are the subject of active research. Previous magmatic intrusion along segments of the rift is indicated by seismic imaging (e.g., Keir et al., 2015; Keranen et al., 2004), and upper mantle seismic structure indicates the presence of partial melt beneath the MER (Bastow et al., 2008; Gallacher et al., 2016). Several of the volcanoes of the MER are deforming (Biggs et al., 2011); deformation is in some cases associated with geothermal activity (e.g., Aluto, Hutchison et al., 2015). Seismicity beneath Aluto volcano is consistent with the presence of a deep (>9 km) magmatic mush zone (Wilks et al., 2017), though a magnetotelluric study suggests that deep magma may be stored 40 km to the west, beneath the Silti-Debre Zeyit Fault Zone and related monogenetic cone field (Samrock et al., 2015).

Hutchison et al. (2015) found a strong structural control on CO_2 degassing on Aluto, with elevated fluxes associated both with a crosscutting regional fault ($\gg$100 g m^{-2} d^{-1}) and the buried caldera rim. CO_2 isotopic values ($\delta^{13}C$ up to $-2.5‰$ in high-flux locations) and their distribution when plotted against the reciprocal of CO_2 concentration that defines a triangular array between magmatic (–3 to $-8‰$), atmospheric ($-8‰$) and biogenic (–20 to $-25‰$) end members suggest that these strong degassing signals likely contain a significant contribution from mantle sources (Hutchison et al., 2016a, and references therein). To date, no other CO_2 flux measurements from the MER have been published.

2. Methodology

2.1. Target Areas for Soil CO_2 Surveys

We targeted localities along the MER for new soil CO_2 surveys, on the basis of proximity to known geothermal sites, to extend our understanding of the links between geothermal activity and diffuse CO_2 flux. An area between the towns of Adama and Sodere (Figure 3f) was surveyed with a sparse (1 km) grid designed to determine the background flux in the center of the rift. The region typifies the central rift, with normal faults (~50 m throw) and an old, buried caldera rim.

The Butajira fault zone (Figure 3b) lies to the east of the towns of Butajira and Silte and encompasses those of Koshe and Tora. Monogenetic cones form a line along the western side of the fault zone and extend further south than most of the faults. The largest faults (80–150 m throw) form a graben west of the Tora-Koshe-Dugda ridge, which reportedly contains a number of hot springs (Ministry of Water Resources [MOWR], 2008).

The Aluto-Langano geothermal field (Figure 3c) is an established resource with active drilling sites. Hutchison et al. (2015, 2016a) showed that the diffuse CO_2 flux here is both substantial and fault concentrated. We extend this survey to the nearby Aluto-Wonji rift flank, which forms part of the Wonji Fault Belt (WFB). The faults form a cascading series of scarps with average trends of ~NNE, commonly segmented and offset by ~NNW trending features. An area of high cone density lies to the northeast of Aluto volcano and to the north of our study area. The Aluto edifice itself is a low-relief, precaldera shield volcano with postcaldera deposits located around the caldera rim and along fault zones (Hutchison et al., 2016a, 2016b). Large volume ignimbrites, possibly from the caldera-forming event(s), have been dated at 306–316 ka, with postcaldera activity (obsidian, pumice, and pyroclastic deposits) occurring between 0 and 60 ka (Hutchison et al., 2016b).

Fentale volcano (alternative spellings: Fantale, Fanta 'Ale) sits at the northernmost end of the rift valley (Figure 3d), as it broadens out into the Afar depression. There are numerous geothermal manifestations both inside the summit caldera and ~15 km to the north (Bekele et al., 2007)—our targeted survey covers Habilo to the NW of the edifice (Figure 3e). Fentale's most recent eruption, in the nineteenth century, resulted in a basaltic lava flow on its southern flank (Gibson, 1974). The vents of the basaltic eruptions align with a trend of ~NNE, possibly suggesting regional, rather than edifice-related, volcanism also indicated by cones to the southwest and north of the edifice.

2.2. Measurement Strategy and Accumulation Chamber Method

Measurements were made by the accumulation chamber method (Chiodini et al., 1998), with a PP Systems EGM-4 Environmental Gas Analyzer for CO_2 and an SRC-1 Soil Respiration Chamber and soil collar (see

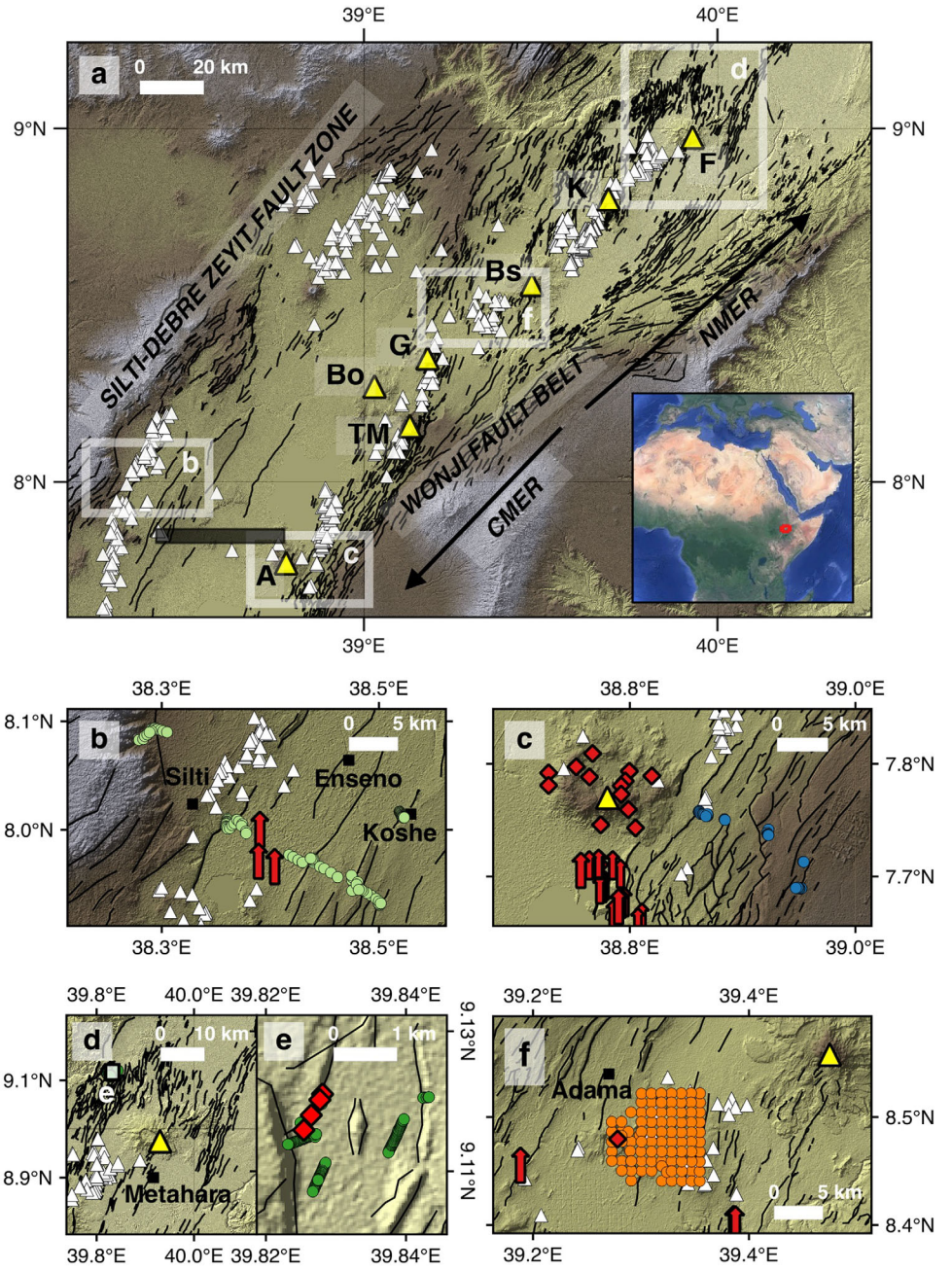

Figure 3. (a) Map of the central and northern Main Ethiopian Rift (CMER and NMER respectively): volcanic cones, white triangles; silicic volcanoes, yellow triangles (A, Aluto; Bo, Bora; Bs, Boset; C, Corbetti; D, Dofen; F, Fentale; G, Gedemsa; K, Kone; and TM, Tulu Moye); black lines delineate faults from the Agostini et al. (2011) database maintained by Giacomo Corti (http://ethiopianrift.igg.cnr.it/corti.htm); elevation from the ASTER GDEM (product of METI and NASA). Semitransparent black bar shows 40 km west of Aluto volcano; approximate location of the conductor identified by Samrock et al. (2015). (inset) Location within East Africa from Google Earth image. (b–f) More detailed location maps as indicated in Figure 3a of the four survey areas: (b) Butajira, (c) Wonji Fault Belt (WFB) east of Aluto (hereafter Aluto-Wonji), (d–e) Fentale and Habilo maps—(e) which is a detail of Figure 3d as indicated, (f) Sodere. Measurement points, filled circles; known hot spring and fumarole locations, red arrows and diamonds respectively. *Sources*: Braddock et al. (2017), MOWR (2008), Geological Survey of Ethiopia and United Nations (1976), and Pürschel et al. (2013); see supporting information Tables 1 and 2.

supporting information). Three campaigns were conducted, each designed with a different aim: (1) the goal of the Sodere campaign was to quantify background flux in the central rift (Figure 3f); (2) the cross-rift, central MER campaign was designed to find and assess areas of elevated CO_2 flux in the regions of Butajira

Table 1
Overview of the Three Campaigns by Survey Strategy: Sodere (Figure 3f), CMER (Central Main Ethiopian Rift, Figures 3b and 3c), and Habilo (Figures 3d and 3e)

Campaign	Date	Type	Approx. spacing (m)	Number of measurements
Sodere	Jan–Feb 2016	Grid	800–1,000	90
CMER (Butajira, Aluto-Wonji)	Jan–Feb 2016	Fault profiles[a]	20–1,000	132
Habilo	June 2016	Fault profiles[b]	10–20	247

[a]Reconnaissance fault profiles across the rift (see text). [b]Targeted fault profiles (see text).

(Figure 3b) and Aluto-Wonji (Figure 3c); and (3) the Habilo campaign was designed as a more focused study on one degassing area (Figures 3d and 3e). In the latter two surveys, profiles were taken across faults to test the hypothesis that high permeability enhances CO_2 flow in such locations. The Habilo campaign afforded the opportunity to decrease the spacing between measurement points, yielding information about the width and flux of degassing at active sites. The influence of seasonal variability on soil gas is untested but expected to be significant due to changes in hydrology and biogenic activity (e.g., Chiodini et al., 2007). In the MER, the main rainy season is from July to September with a minor rainy season from April to May. The campaigns were conducted within the dry seasons. Table 1 outlines the survey type, number of measurements and average spacing for each campaign.

2.3. Compilation of Hot Spring and Fumarole Locations

To constrain the frequency and distribution of degassing areas along the rift, and investigate the structures controlling CO_2 emission, we reviewed the locations of hot springs and fumaroles in the MER (supporting information Table 1).

A number of surveys have attempted to catalogue geothermally active regions in the MER (e.g., Abiye & Haile, 2008; Ayele et al., 2002; Di Paola, 1970; Teclu, 2002). The first of these was conducted by the United Nations Development Programme (UNDP) (1973), combining field work and a helicopter-borne infra-red survey across an area from Lake Abaya in the south to the Danakil Depression in the far north. Subsequent studies confirmed and extended this regional directory (e.g., Haile Selassie, 1984), while others have focused on the geology and/or hydrology of smaller areas of interest (e.g., Ayenew et al., 2008; Bekele et al., 2007; Beyene, 2000; Kebede et al., 1985; Rampey et al., 2010; Stadler et al., 2007; Williams et al., 2004). Many of these reports represent research conducted by industry (e.g., Reykjavik Geothermal; Gislason et al., 2015) or government departments (e.g., Geological Survey of Ethiopia/Ministry of Water and Resources, often in partnership with UNDP), and remain in the grey literature (see supporting information Table 1). Also included are two Master's reports, focusing on the Tulu Moye area (Bahiru, 2007; Mengistu, 2016). Many reports do not publish grid references, so locations were obtained by map comparison and/or from field descriptions. Errors up to 5 km are common, however, this does not prevent an appraisal of known geothermal areas in most cases.

Table 2
Results From the Three Campaigns

Area	Number of measurements	Mean flux (g m^{-2} d^{-1})	Standard deviation
Sodere	90	21.9	9.3
Butajira	88	28.7	34.7
Aluto-Wonji	44	10.6	6.4
Habilo	247	157.3[a]	401.3[a]

Note: For breakdowns by fault, see supporting information Table 3. High-flux values in Habilo and Butajira create a large positive skew in the data; standard deviation is therefore higher than the mean.

[a]Represents an underestimate—some values exceed measurement limit (2,400 g m^{-2} d^{-1}).

3. Results

3.1. Soil CO_2 Survey

CO_2 survey results from each of the four areas are summarized in Table 2 and Figures 4 and 5. The measurement limit of the instrument is 2,400 g m^{-2} d^{-1}; only the Habilo area exhibited sites that exceeded this limit. Habilo shows the greatest average flux over all sites, and greatest variation as shown by standard deviation. The Aluto-Wonji measurements are the lowest and most consistent, with the majority of flux values <10 g m^{-2} d^{-1}. Butajira and Sodere areas share a similar mean flux (20–30 g m^{-2} d^{-1}) but the variation in flux from Butajira greatly exceed those from Sodere (Figure 4). Frequency analysis of the data depends significantly on the measurement strategy—our hypothesis is that CO_2 degassing is closely restricted to near faults, so it is unsurprising that the sparse grid employed for the Sodere area fails to resolve the higher flux values, limiting its variability. The Butajira survey targeted faults using sampling transects and

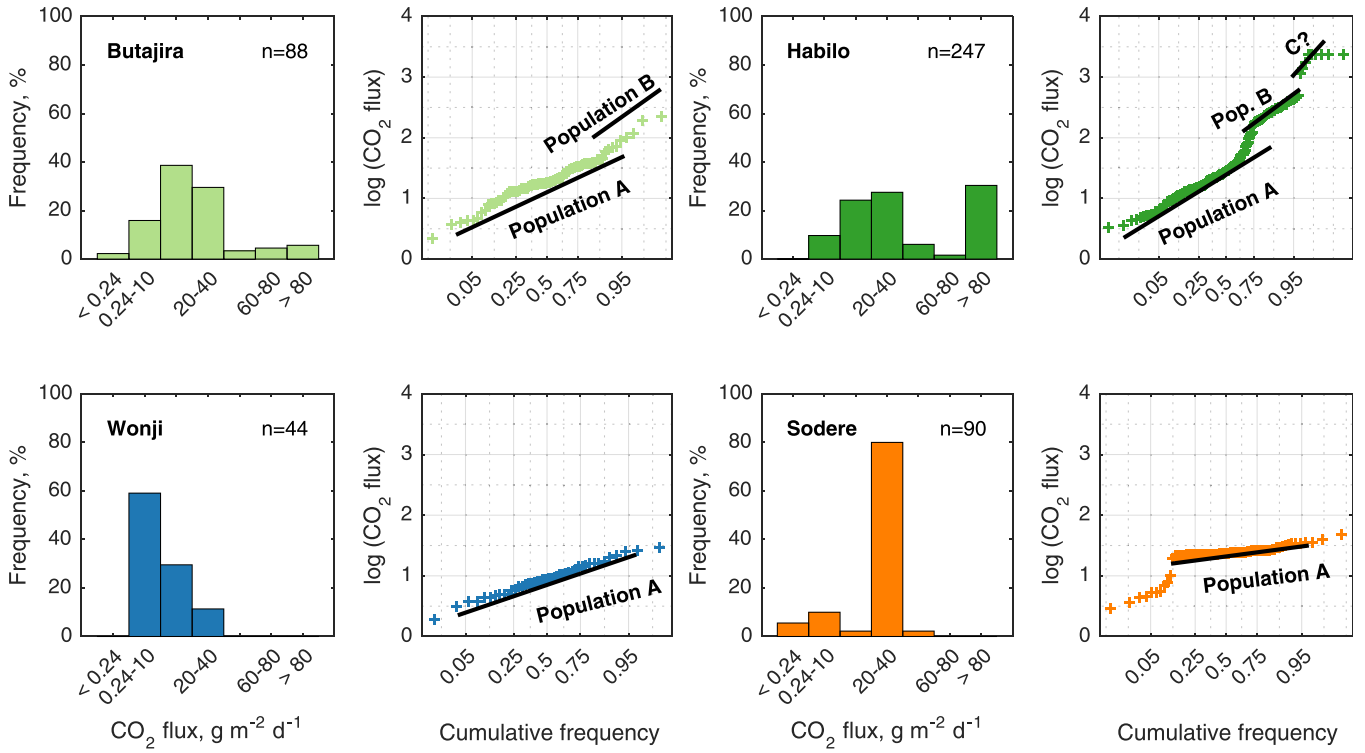

Figure 4. Histograms and cumulative frequency plots of each target area. The Wonji measurements exhibit only one population (A) representing background flux, whereas Butajira and Sodere show probable contributions from areas of elevated diffuse degassing (B). Habilo exhibits concentrated degassing along faults (B) and possibly a distinct population provided by fumaroles and their immediate vicinities (C).

smaller spacing—and is therefore more likely to encapsulate a higher variability. One implication of this interpretation is that the Sodere region could be analogous to Butajira, but a more targeted survey is needed to test this hypothesis.

The relative contribution of different CO_2 sources can be distinguished at least to some extent using cumulative frequency plots (e.g., Cardellini et al., 2003). An inflection in the plot implies different frequency behavior in a set of measurements, and therefore two overlapping populations—a single population would

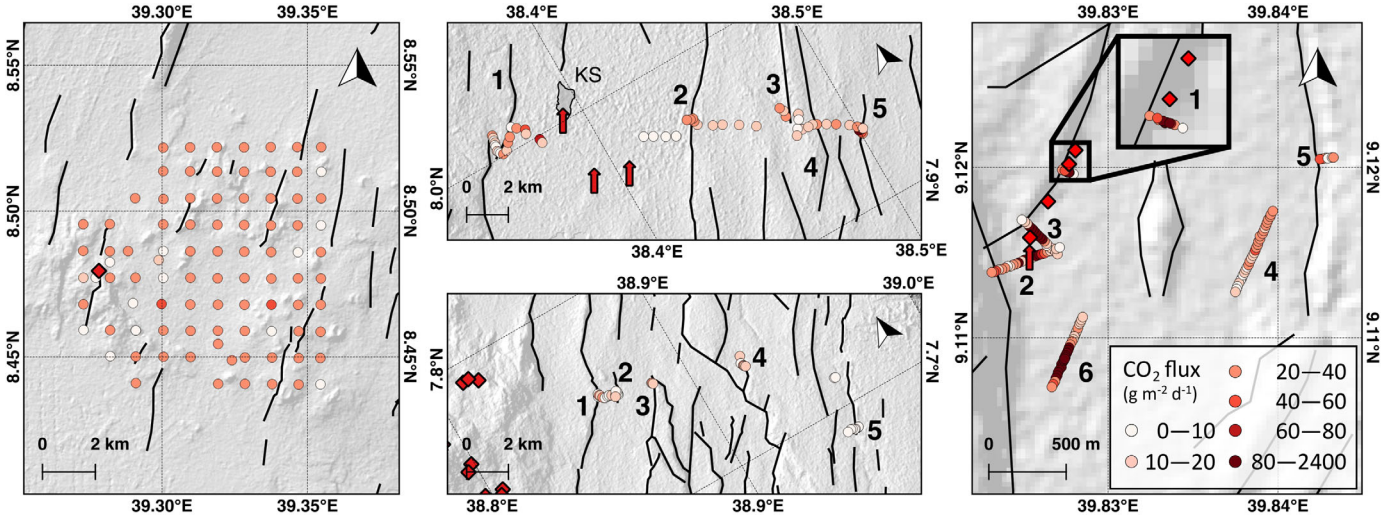

Figure 5. Maps showing flux results across four campaigns. (left) Sodere, (top) Butajira, (bottom) Aluto-Wonji, and (right) Habilo. Red arrows and diamonds represent hot springs and fumaroles respectively. Profile lines have been numbered. KS = Kuntane swamp. Faults from the Agostini et al. (2011) database (http://ethiopianrift.igg.cnr.it/corti.htm).

appear as a straight line. The example of Habilo is clearest, with an inflection at a flux of around $10^{1.5} \approx 30$ g m^{-2} d^{-1}. We suggest that, for these campaigns, a value of >30 g m^{-2} d^{-1} represents an "elevated" value, associated with a significant contribution from an additional/different source. The background contribution to the soil CO_2 flux is biogenic carbon, with a typical flux of 0.2–50 g m^{-2} d^{-1}, rising to 100 g m^{-2} d^{-1} in some areas, depending on the type and density of local vegetation and soil (e.g., Chiodini et al., 2008; Hernández et al., 2012; Hernández Perez et al., 2003). Our choice of cutoff value, on the basis of frequency analysis of our data, is higher than previous studies in similar locations (e.g., 6 g m^{-2} d^{-1} for Aluto; Hutchison et al., 2015) but is consistent with soils in less arid climates (e.g., Cardellini et al., 2003; Chiodini et al., 2008). We use this cutoff value to argue for the presence (or lack) of deep CO_2 flux only; our estimate of total CO_2 flux is independent of this value (see section 4.3.1).

The close association between fumaroles and elevated soil gas fluxes (10^3 to 10^4 g m^{-2} d^{-1}) points to a common volcanic/hydrothermal origin (see Figure 4), and on this basis we propose a deep origin for the majority of elevated values across the four areas. Carbon-isotopic analysis would be useful to confirm this conclusion, as shown in Aluto and the Magadi and Natron basins (Hutchison et al., 2016a; Lee et al., 2016).

The Aluto-Wonji survey found no elevated values, while the Habilo survey has a strong signal assumed to be of magmatic origin. The use of high resolution profiles across faults enables further consideration of the nature of CO_2 flux in the areas surveyed, discussed in section B of the supporting information.

3.2. Map of Hot Springs and Fumaroles

Figure 6 is a map of known hot springs and fumaroles, based on our literature survey, including error estimates on the location (section 2.3, supporting information Tables 1 and 2). Active areas are aligned NE-SW along a straight line, seemingly independent of the change in rift trend from NNE-SSW in the south to NE-SW further north. Butajira and the Bodicho Springs are located off axis to this general trend (Figure 6 and supporting information Table 2). The southernmost region of the study area is anomalous (Figure 6), with isolated hot springs distributed along the Bilate River with possible structural associations with old volcanic centers (e.g., Data and Ashire volcanoes; UNDP, 1973). Rift architecture changes south of Lake Awassa; the southern MER represents an early stage of rift evolution in which border faults still accommodate strain (Agostini et al., 2011), possibly influencing the distribution of magmatism and associated geothermal areas (Bastow et al., 2005; Muirhead et al., 2016).

Most active regions can be separated into two categories: volcanic, fumarole-dominated systems (e.g., Aluto, Corbetti, and Fentale); and regional, hot spring-dominated systems (e.g., Habilo, Filoa, Hippo Pool, Sodere, and others). Hot springs are common near some lakes (e.g., Abaya, Shalla, and Langano) but absent near others (e.g., Abijata, Awassa, and Koka). Many regional systems are possibly related to volcanic centers, e.g., Habilo, Filoa and Hubicha near Fentale and Doredimtu, Wondo Genet and Graha Quhe near Corbetti. The relationships between Hippo Pool (and Gargadi Spring), Boku and Sodere Springs is unclear, as are the influences of the Gedemsa and (older) Boku/Sodere caldera on these features.

Most studies do not systematically record spring geochemistry, and further work is recommended. Hot springs vary in temperature with values commonly around 40–60°C, higher temperatures reach 80–100°C (e.g., 81.5°C, Habilo; Bekele et al., 2007; 82°C, Langano; Pürschel et al., 2013; 95°C, Chokore; UNDP, 1973).

4. Discussion

4.1. Diffuse Degassing in the Main Ethiopian Rift

The irregular spacing and scarcity of data from the CMER and Sodere campaigns suggest that these results cannot be used to quantify the CO_2 flux from the elevated flux areas, however, they do help to constrain the distribution of areas with elevated flux, and therefore the nature of degassing across the MER. In both the Habilo and Butajira areas, some faults concentrate CO_2 release and others do not. There is no evidence for elevated CO_2 release along Wonji faults observed to the east of Aluto, though the number of measurements is low and along-strike variation in degassing cannot be discounted.

The results of the soil CO_2 surveys in Habilo, Butajira, and Aluto-Wonji are in concordance with the distribution of hot springs, fumaroles, and other geothermal manifestations in each area (Figure 6). The results have implications for our understanding of degassing through rift structures. The magnitude of CO_2 flux varies

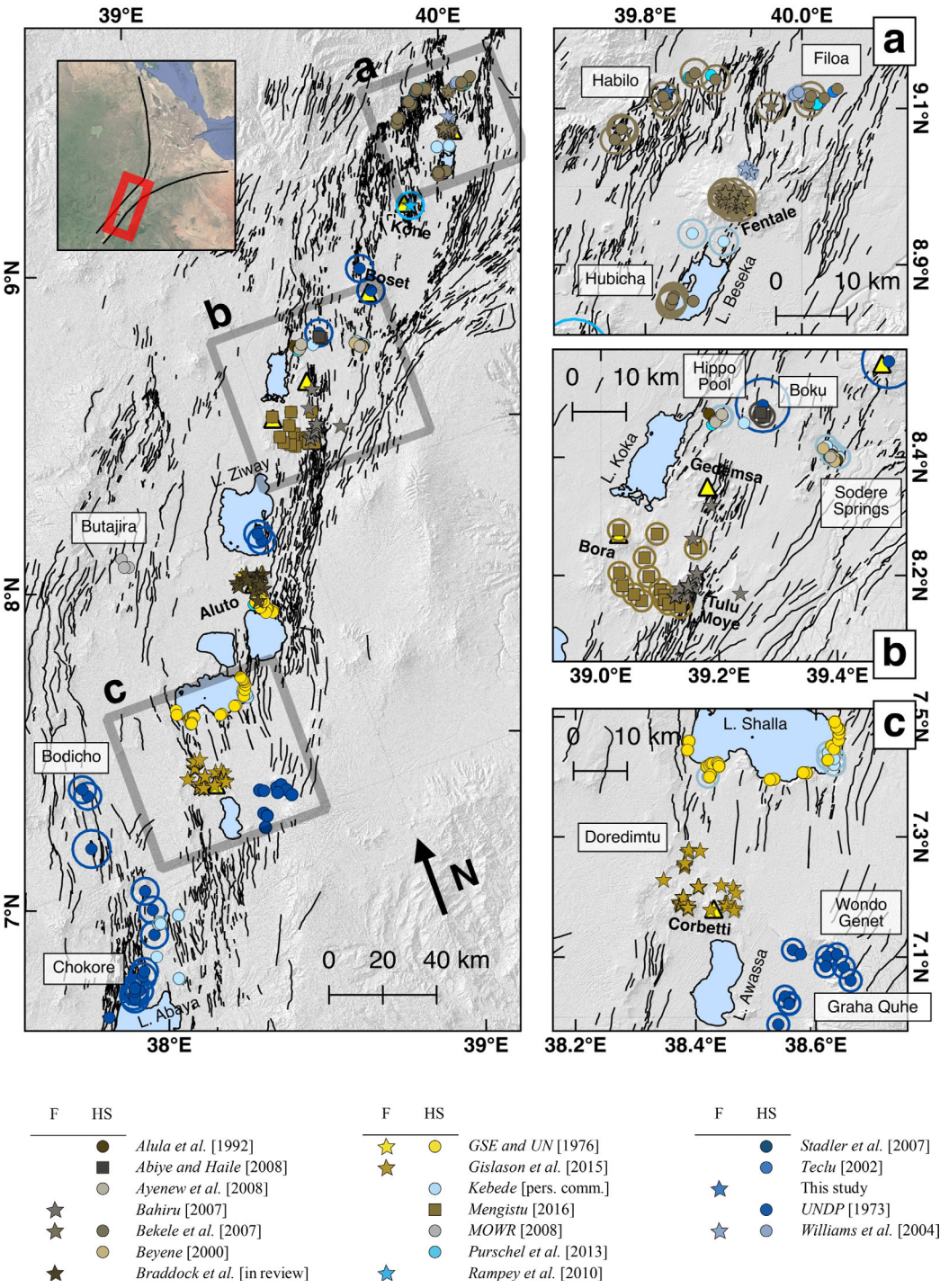

Figure 6. Map of fumaroles (stars), hot springs (circles), and reports of fumarolic areas/warm ground (squares) compiled from various data sources (see supporting information Table 1). Estimates of error in location are shown by hollow circles. Notable sites of off-edifice activity are labeled, shown in more detail in insets (a–c). (inset) Location within MER from Google Earth image.

on three spatial scales, which we consider in turn. First, variability within degassing profiles (section 4.1.1). Second, variability within areas of high CO_2 flux, since only certain faults concentrate gas flow (section 4.1.2). Finally, we assess variability along the MER, and discuss implications for magma storage regimes and rift-scale CO_2 emissions estimates (section 4.1.3). Notably, we have not attempted to constrain the temporal variability in diffuse degassing, which remains a high priority for future work.

4.1.1. Profile-Scale Variability

Soil gas surveys in the MER show that CO_2 flux varies significantly over a length scale of tens of meters, as observed in many other areas worldwide (e.g., Chiodini et al., 1998; Lee et al., 2016). The width of the area through which gas flow is concentrated, and the variability of the flux within this area, dictates the appropriate spacing between measurements in surveys of this kind. Since the width of degassing signals can be as little as 50 m (HF1, Figure 7), the spacing between measurements must be less than 50 m in order to not miss such signals. In the cross-rift campaign (Butajira and Aluto-Wonji), measurement spacing was reduced to 20–50 m near faults. In the targeted Habilo campaign, measurement spacing was reduced further to 10–20 m, in an attempt to capture the shape of the degassing signal and within profile variability (see Table 1 and supporting information section B).

Within areas of high CO_2 flux, high-flux variability is observed on short (<20 m) spatial scales (e.g., HF6; Figure 7, right), and order of magnitude variations in CO_2 flux have been reported on a scale <1 m in highly altered environments elsewhere (e.g., Chiodini et al., 1998). The profiles from the Habilo graben show

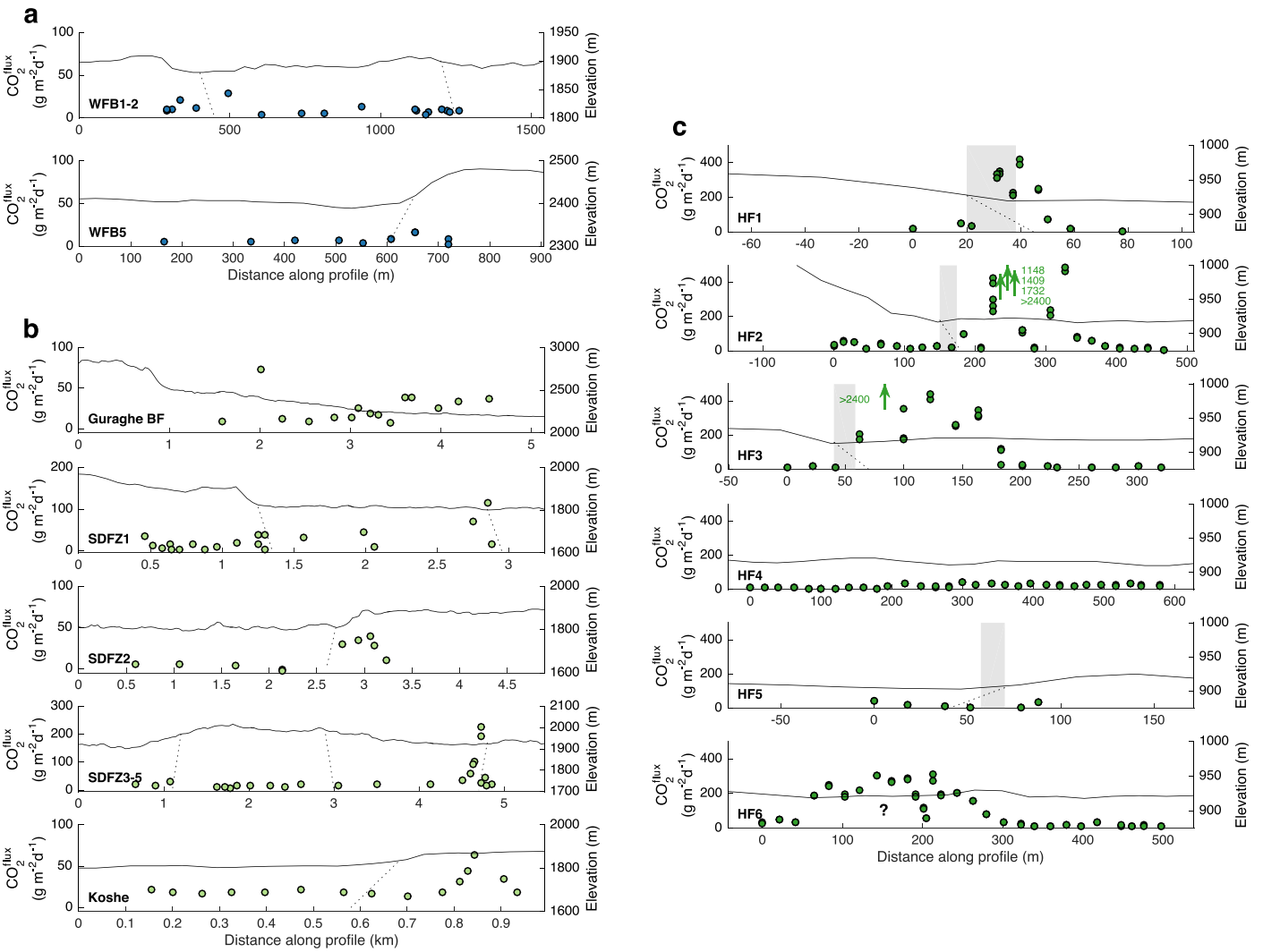

Figure 7. Selected profiles across faults. Fault/profile numbers are shown on Figure 5, names are derived from appending a regional code (SDFZ, Silti-Debre Zeyit Fault Zone; WFB, Wonji Fault Belt; and HF, Habilo-Fentale). Shaded grey areas represent a fault zone based on the faults maximum throw. The throw is calculated using the fault-throw relationship in the same manner as Lee et al. (2016). (top left) No elevated flux is observed across Wonji faults. (bottom left) SDFZ2 and SDFZ5 show elevated flux, while others do not. SDFZ1 represents a large offset fault with no significant carbon release. Further work is needed to investigate (top) the Guraghe border fault; any elevated flux must be spatially restricted. (right) Very high flux is observed along the western side of the Habilo graben (HF1–3); none is observed on the eastern side. An elevated profile is recorded across HF6, with little/no topographic expression of faulting. Elevated flux bears little correlation to fault zones.

multiple variations away from a first-order smooth curve, with flux varying by a factor of two within 10–20 m. Quantification of the magnitude of the flux from these sites requires multiple measurements at a high spatial density (at least 5–10 m) to ensure surveys capture the first-order variability. This high spatial density of measurements precludes the use of popular techniques such as Sequential Gaussian Simulation (SGS; e.g., Cardellini et al., 2003) for rift-scale estimates. SGS provides a smooth-varying probability of exceedance from which diffuse degassing structures may be identified and total fluxes estimated, but it requires a regular measurement grid for interpolation. In the absence of such techniques, we fit Gaussian curves to the profiles from the Habilo graben to estimate the total flux from this area (section 4.3.1). More advanced statistical techniques would be a profitable area for future research.

Point source fluxes from fumaroles/hot springs that exceed the measurement limit are difficult to include in total estimates (see Population C from Habilo, Figure 4). On Etna, Giammanco et al. (2007) sampled both focused and diffuse degassing manifestations from mud volcanoes and showed that the net flux from focused sites were 2–3 orders of magnitude lower than sites of significant diffuse degassing.

The difference in scales between gas flux variation and the area of interest (the width of the rift, ~50 km) presents the central difficulty in constraining rift-scale CO_2 degassing. Surveys of high spatial resolution necessarily focus on degassing areas, and the proportions of degassing to non-degassing areas are left uncertain.

4.1.2. Basin-Scale Variability

The Habilo and Butajira areas both exhibit elevated flux, however, some faults concentrate degassing whereas others do not. The extent to which a fault will act as a conduit for gas release depends not only on size but also on its permeability and geometry.

Fault permeability represents a major control on fluid transport and is a function of many parameters including lithology, mean stress, and recent activity (e.g., Faulkner et al., 2010; Sibson, 2000). In the Butajira region, the Guraghe border fault did not exhibit a wide degassing signal (Figure 7a). One single elevated value was measured, ~1.5 km west of the expected fault trace. While the maximum throw of the Guraghe border fault is >1 km, there is no evidence for degassing from the fault zone across a similar length scale. While large faults may create wider damage zones of increased permeability, and fluid transport, the ability of a fault to enhance the CO_2 flux will also depend on recent activity. Studies in Italy and the KRV suggest a close relationship between strain rate and fluid flow (Camarda et al., 2016; Muirhead et al., 2016). The time since rupture influences the degree of fault resealing, and is a significant control on porosity. Border faults like the Guraghe fault are large but inactive, and their permeability may therefore be low. The smaller faults that appear to concentrate degassing in the Butajira region may be more recent and active, creating efficient conduits through which CO_2 may flow. In contrast to the Natron basin (3 Ma), the older Magadi basin (7 Ma) is analogous to the MER in this respect: it has reduced border fault activity and increased activity toward the rift center, leading to enhanced degassing in this location (Muirhead et al., 2016).

Fault geometry with respect to the source may also control fluid transport. In the Habilo region, we found elevated degassing along the eastward-dipping faults on the western side of the basin, associated with a line of fumaroles. The westward-dipping fault, on the other hand, displays no elevated flux. The eastward-dipping faults of the Habilo graben may therefore exploit a source to the east more effectively, the location of which is the subject of surveys conducted by Hotspur Geothermal. This observation has important implications for which faults we expect to concentrate CO_2 flux—those actively concentrating CO_2 flux can be separated from those that do not by only 1–2 km. The detailed structural associations of degassing are therefore important to account for in estimating a net flux from an active basin. The presence of hot springs and fumaroles provide a first-order assessment of emission along structures.

4.1.3. Rift-Scale Variability

Our surveys also shed light on the distribution and limits on areas of CO_2 emission along the rift. Despite their proximity to the actively degassing Aluto-Langano geothermal field, the Wonji faults to the east of Aluto show no evidence of elevated CO_2 flux (Figure 8). Although the number of measurements is smaller than other areas ($n = 44$), and degassing along-strike or on different faults cannot be discounted, a lack of high CO_2 flux (i.e., >40 g m^{-2} d^{-1}) in the WFB zone close to Aluto volcano and the distribution of hydrothermal manifestations (Figure 6) suggests that the CO_2 source is spatially restricted. Fumaroles are found almost exclusively on the Aluto edifice itself and associated hot springs are located to the south (Figure 6). This may reflect local hydrology: Lake Ziway is not connected to Aluto's hydrothermal circulation, or to

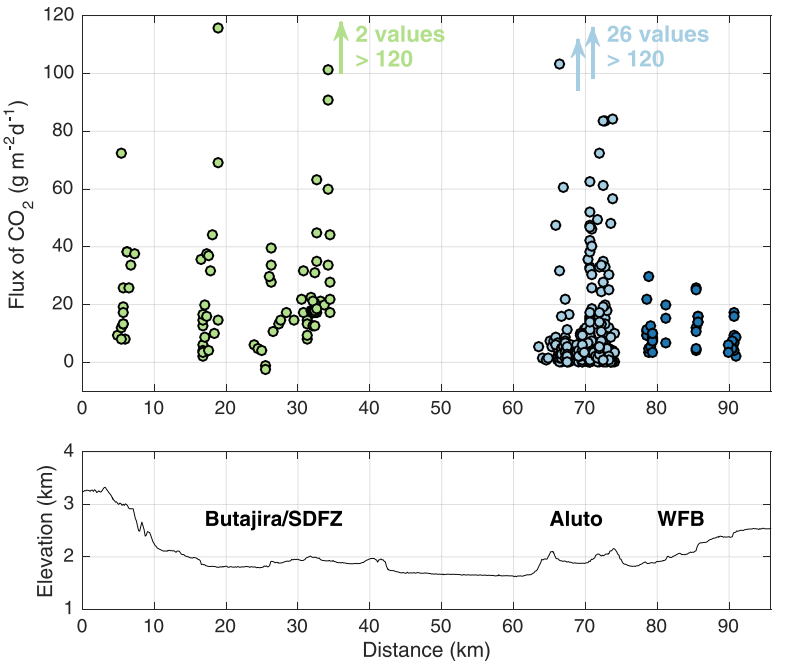

Figure 8. Cross-rift profile showing asymmetric degassing in the central MER, through Butajira/Silte Debre Zeyit Fault Zone (SDFZ; pale green), Aluto (pale blue; data from Hutchison et al., 2015), and the Wonji Fault Belt (WFB; dark blue). Diffuse degassing is evident on the western side of the rift as well as focused on Aluto volcano. The Wonji Fault Belt immediately east of Aluto shows no evidence of elevated flux, suggesting a restricted flow field.

groundwater flowing into Lake Langano in the south (Darling et al., 1996). Areas to the north and east are therefore not able to access the restricted CO_2 source beneath the volcanic edifice, whereas the flow of water southward extends the geothermal field in this direction (Hochstein et al., 2017).

In contrast to these results on the eastern side of the CMER, the Butajira survey suggests fault-controlled degassing along certain faults. Elevated flux is observed in the central graben near the fault-aligned Kuntane swamp and associated hot springs, while the highest flux is recorded along a fault trace difficult to identify in the field (Figure 5, top). There is evidently a source of CO_2 available to these faults. The deep conductor predicted from magnetotellurics ~40 km west of Aluto (Samrock et al., 2015) would lie approximately beneath the Tora-Koshe ridge (Figure 8). Magma storage offset from the main rift axis (along which the majority of geothermal, volcanic, and seismic activities lie) is therefore a likely CO_2 source for the Butajira area.

The storage of magma away from volcanic edifices may be an important feature of the rift. Monogenetic volcanic fields are distributed throughout the MER, with notable cones around the towns of Butajira and Silte (Figure 3). Field stratigraphy suggests that many of these cones are young, which implies an ongoing risk of eruption from locations away from the main volcanic centers.

The prevalence of off-edifice degassing in continental rifts could be considered evidence toward the widespread potential for regional volcanism. While mantle-derived magmas may be arrested at depth, repeated intrusion into extending crust may be accompanied by occasional surface volcanism. The new observations of CO_2 degassing from the Butajira and Habilo sites, along with that from the Magadi and Natron basins (Lee et al., 2016) and the magnetotellurics study west of Aluto (Samrock et al., 2015), suggest that further investigation of magma storage and volcanic risk in areas which have already shown signs of magmatic intrusion would be worthwhile (cf., Biggs et al., 2009; Ibs-von Seht et al., 2001; Keranen et al., 2004; Roecker et al., 2017).

4.1.4. Summary of Diffuse Degassing in the Main Ethiopian Rift (MER)

Degassing in the MER is not continuous throughout the rift, but is instead spatially restricted to degassing sites that include both historically inactive volcanoes and off-edifice sites. Extrapolation of fluxes to the rift-scale must account for the patchy nature of degassing within continental rifts. Within each measured site,

some faults concentrate CO_2 flow and others do not. The identification of active structures that act as efficient fluid pathways is therefore important. The magnitude of emissions varies within zones of elevated CO_2 flux. The inherent variability on all scales and the small footprint of diffuse degassing measurements relative to potential degassing structures create difficulties when estimating a rift-scale CO_2 flux.

4.2. Areas of Geothermal Activity in the MER

Having discussed the variability in diffuse CO_2 degassing along the rift, we turn now to the broader identification of geothermal areas throughout the MER as manifested by hot springs and fumaroles. First, the new database must be appraised, before the distribution of active areas is discussed and compared to the KRV.

4.2.1. Appraisal of Database

Given the scope and frequency of large studies such as that of the UNDP (1973), in addition to the socioeconomic interest shown in areas of geothermal activity and high population density, it is unlikely that there are large areas yet to be explored. However, isolated hot springs and/or fumaroles in remote areas may be unreported. Though we expect most general areas to be in some way documented, the number of specific locations for each area varies greatly and is strongly affected by the number of existing studies. For example, though a number of reports mention fumarolic activity in the Boset Volcanic Complex (e.g., Haile Selassie, 1984; UNDP, 1973), we do not find any confirmed locations of geothermal manifestations in the literature beyond field descriptions. It is nevertheless likely that Boset is a geothermally active volcanic system (M. Siegburg, personal communication, 2017) and it is included in the following discussion accordingly. In contrast, Gedemsa volcano is within the study area of several reports and has been noted as absent of current geothermal manifestations (Abera et al., 2014; Alula et al., 1992; Bahiru, 2007; Thrall, 1973). Fumaroles may be underreported compared to hot springs as they are often smaller, more remote and not targeted for hydrogeochemical analysis, although they may be focused in and around volcanic centers unlike hot springs that may be more widespread.

A number of caveats must be stated for using hot spring/geothermal feature locations as a proxy for geothermal activity, and by extension CO_2 emissions. Incidences of large CO_2 flux apart from associated geothermal features (cold, dry vents) have been reported in many regions globally, though not in the MER, e.g., Hokkaido, Japan (Hernández Perez et al., 2003), Lake Kivu, DRC (Smets et al., 2010), Mammouth Mountain, USA (Sorey et al., 1998), and Rungwe Volcanic Province, Southern Tanzania (Barry et al., 2013; de Moor et al., 2013). Hot springs are also intimately tied to local hydrology. Their locations are therefore biased toward lakes, rivers and areas of shallow groundwater. This may explain the relative abundance of features in the central MER (Lakes District) compared to the northern MER (Awash basin, Boset-Fentale).

Well-known sites of geothermal interest are included in many data sets (e.g., Hippo Pool, Sodere Springs), leading to a duplication of these locations within the combined catalogue. The errors in location prevent us from identifying these duplicates beyond doubt. Geospatial analysis concerning the density and alignment of features is therefore precluded by the presence of duplicate features, the errors in location and the uncertainty in the completeness of the final database. The value of the database is in the identification of geothermally active areas and their relationship with tectonic and volcanic features. A comprehensive record of temperatures and geochemistry of springs and fumaroles across the Main Ethiopian Rift would help to assess the geothermal activity of each area. The compilation presented here represents the first step toward this goal.

4.2.2. Characterizing CO_2 Source Areas

As noted in section 3.2, the majority of geothermal areas in the MER are found along a NE-SW line and can be divided into two categories: edifice-based, fumarole-dominated systems relating to Holocene volcanic centers and off-edifice, hot spring-dominated systems which may or may not be interconnected at depth (Figure 6). The distance from Butajira and the Bodicho Springs to the nearest Holocene volcanic centers implies separate heat sources for these features, and therefore the possibility of magma storage offset from the main rift axis. Most manifestations are coincident with structural features (see supporting information Table 2), underlining the role of fault networks in heat and fluid flow.

The MER is an area of high geothermal activity and, while the local population benefit from hot spring resorts (e.g., Sodere Springs and Wondo Genet) and the country benefits from energy production (e.g., Aluto and Corbetti), hazards must also be assessed. Fluoride concentrations in drinking water are often above guidelines presented by the World Health Organization, and are attributed to the high rate of CO_2

outgassing (e.g., Gizaw, 1996). The Fentale area in particular hosts several manifestations of hydrothermal activity both on-edifice and off-edifice and is one of the most seismically active regions in the rift (Keir et al., 2006), warning of the potential for seismic and volcanic hazards. Similarly, the abundance of hot springs around the O'a caldera coupled with seismic activity and the unknown present state of volcanic unrest suggest a high priority for future work on Lake Shalla and the underlying volcanic complex (Mohr et al., 1980).

Though the magnitude of degassing likely varies substantially between active geothermal areas, the compilation map (Figure 6) provides a first-order view on the distribution and frequency of such areas. By assuming a range of CO_2 fluxes from each type of area (on-edifice or off-edifice) and extrapolating along the rift, an estimate for rift-scale degassing can be found (section 4.3.1).

4.3. Estimating Rift-Scale Carbon Flux

In scaling up from their measurements of the Magadi and Natron basins, Lee et al. (2016) categorized their survey area into three structural zones (hanging wall, footwall, and fault zone) using aerial and satellite imagery, supplemented by field mapping. They defined the fault zone as an area of width equal to the maximum fault throw (see Figure 7), and estimated the flux from the total zone area in each basin (Magadi and Natron) multiplied by the mean CO_2 flux for each zone. Lee et al. (2016) noted the sparse sampling used in regional surveys, and the errors associated with assuming a fair distribution of sampling within these structural zones. In their extrapolation to the entire Eastern Rift they calculate a mean flux per area for the segment of the rift in which the basins are located (from Oldoinyo Lengai to Suswa volcano). The segment area is 9,200 km^2 (184 km long $\times$ 50 km wide), ten times the combined areas of the basins surveyed (982 km^2, see Figure 9). The flux per unit area within the Magadi and Natron basins is 3,900 and 4,300 t km^{-2} yr^{-1}, respectively. Assuming emissions within the segment are solely from the Magadi and Natron basins, the mean flux per area drops to 440 $\pm$ 206 t km^{-2} yr^{-1} across the entire segment. Assessment of the spatial frequency of areas such as the Magadi and Natron basins would help to constrain this estimate. Extrapolation of a mean flux of 440 $\pm$ 206 t km^{-2} yr^{-1} along the entire Eastern Rift (comprising KRV and MER; 3,240 $\times$ 50 km) yields an estimate for a total flux of 71 $\pm$ 33 Mt yr^{-1}. Lee et al. (2016) called for further surveys along the Eastern Rift to better constrain this extrapolation. Here we use our observations from the MER (section 4.3.1) to evaluate the outgassing flux, and explore possible CO_2 sources that might account for this flux (section 4.3.2).

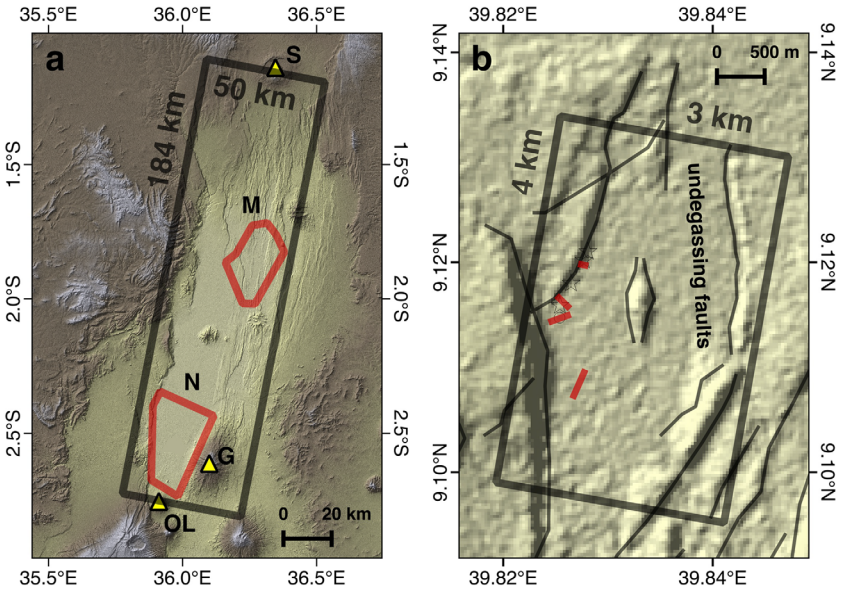

Figure 9. (a) Scaling argument from Lee et al. (2016). Emissions from the Natron (N) and Magadi (M) basins are averaged over a segment of the rift (taken to be 50 km wide), the along-rift length of which is limited by Oldoinyo Lengai (OL) and Suswa volcano (S). (b) Simple estimate for CO_2 emissions from the Habilo graben. The faults on the western side are degassing, whereas our data provides no evidence of elevated flux elsewhere. Assuming a mean width and magnitude of elevated flux, a total degassing figure can be estimated (see section 4.3.1, Table 3).

4.3.1. CO_2 Emissions From the Main Ethiopian Rift

We estimate the rift-scale degassing by combining our new surveys (section 4.1) with the distribution of geothermal areas in the MER (section 4.2). The CO_2 flux from a degassing area is estimated, and the total flux from the Main Ethiopian Rift is extrapolated on the basis of the spatial frequency of geothermal areas following our observation that CO_2 flux correlates with geothermal activity (section 4.1). This remains a hypothesis to test in future surveys. Extrapolation to the entire Eastern Rift is provided for comparison with previous estimates.

The total load from Habilo can be estimated by considering the flux of CO_2 from the western side of the graben (Figure 9b). We find no evidence for degassing on the eastern side, though along-strike variation cannot be ruled out. The major, CO_2-concentrating fault exhibits fumaroles and hot springs, and elevated degassing across a width of 25–275 m (Figure 7c). The elevated signal is here modeled as a Gaussian curve for profiles HF1, HF2, HF3, and HF6 (see Figure 10). Profiles HF1, HF3, and HF6 provide close fits despite small-scale variability (likely due to permeability variations in the near subsurface, see section 4.1.1). HF2 requires two Gaussian curves, although it is unclear whether this signal represents two elevated regions or one with higher variability. Owing to this uncertainty, confidence bounds are too broad for a useful estimate and are not used in further calculations.

The curves do not include values recorded in the immediate vicinity of fumaroles and hot springs (often beyond the measurement limit of the instrument). The relative contribution of these point sources compared to that from the faults is unclear (see section 4.1.1). The following discussion therefore deals only with diffuse degassing. The integrated area beneath the Gaussian curves, resolved perpendicular to the local fault strike, represents diffuse CO_2 flux per unit length of the CO_2-concentrating fault. We do not

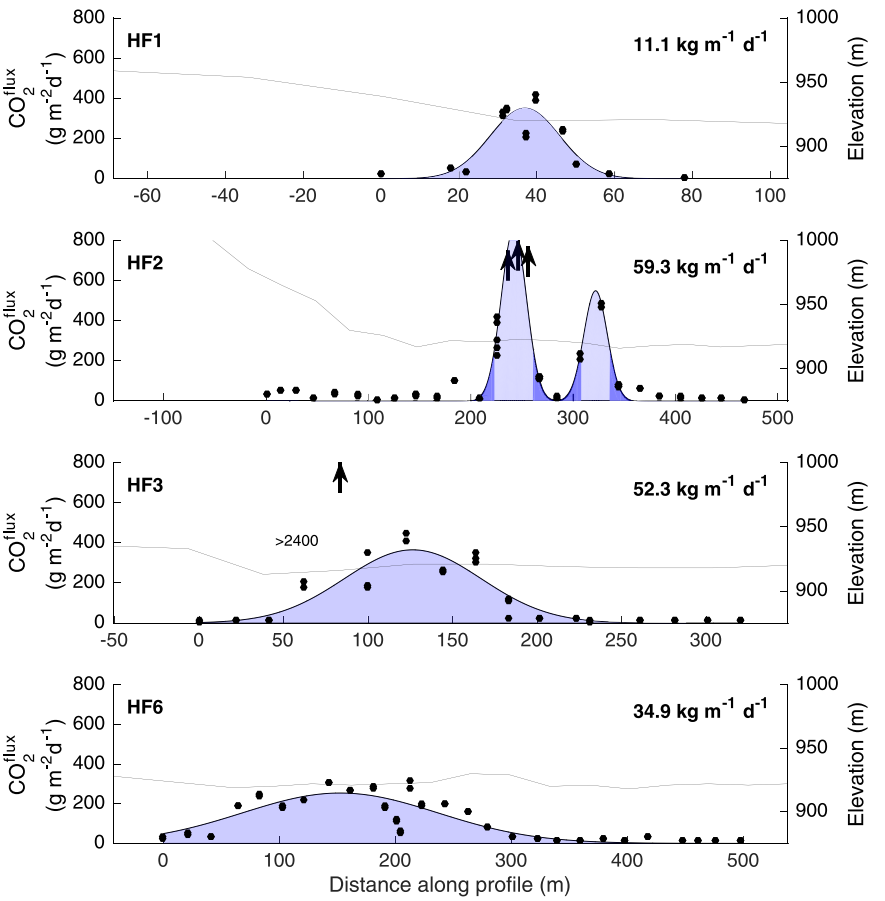

Figure 10. Degassing profiles from the Habilo survey, along the western boundary of the graben. Best fit Gaussian curves are shown—the area under the curves represents the estimates of CO_2 flux per unit length along the degassing fault from each profile (see Table 3).

Table 3
Estimates for the Along-Strike CO_2 Flux From the CO_2-Concentrating Faults of the Habilo Basin, Extrapolated From Profiles HF1, HF3, and HF6 Assuming a Degassing Fault Length of 4 ± 2 km

Fault	CO_2 flux per length of degassing fault (kg m^{-1} d^{-1}, 95% confidence bounds)	Total estimated load from Habilo (kt yr^{-1})
HF1	11.1 (7.4–15.5)	16.2 (5.4–33.9)
HF3	52.3 (36.6–70.8)	76.4 (26.7–155.0)
HF6	34.9 (25.8–45.3)	51.0 (18.9–99.3)

Note: HF2 is not included in analysis owing to uncertainty in fitting a Gaussian curve.

account for the biogenic carbon flux on the basis of a cutoff value, but assume all degassing is magmatic. The approximate error associated with this assumption is <10 kg m^{-1} d^{-1}, given the maximum observed width of the signal (275 m) and the biogenic cutoff value from frequency analysis (30 g m^{-2} d^{-1}). If we assume a degassing fault length of 4 ± 2 km (see Figure 9b), the total load is estimated as 5–155 kt yr^{-1} (see Table 3).

Scaling up to quantify the rift-scale CO_2 degassing flux requires an estimate of the number of degassing fields. We separate geothermal degassing sites (section 4.2), into on-edifice and off-edifice. Most geothermal energy prospects in Ethiopia are centered on volcanic edifices (Kebede, 2012), and we obtain an upper estimate of the flux from these sources by assuming that the 5–7 volcanic areas (Fentale, Boset, Tulu Moye, Aluto, and Corbetti) each release a diffuse CO_2 flux similar to that measured for Aluto volcano (90–180 kt yr^{-1}; Hutchison et al., 2015). O'a caldera feeds multiple hot springs, and is clearly degassing; the status of Kone Volcanic Complex is uncertain. This yields a total volcanic flux of 0.45–1.26 Mt yr^{-1}.

We use Habilo (5–155 kt yr^{-1}) as a representative of the off-edifice areas along the rift. Further surveys of off-edifice sites are required to assess how robust this assumption is. Habilo contains a single hot spring (81.5°C; Bekele et al., 2007) and numerous fumaroles and dried mud pools, suggesting greater geothermal activity than elsewhere (e.g., Hippo Pool, 35–47°C; UNDP, 1973). From our compilation of geothermal locations, we estimate that there may be 14–20 off-edifice geothermal areas (see Table 4), yielding an estimate for off-edifice degassing of 0.07–3.10 Mt yr^{-1}.

Combining edifice and off-edifice areas, the total diffuse CO_2 flux along the central and northern MER (from the north coast of Lake Abaya to Fentale volcano) is estimated at 0.52–4.36 Mt yr^{-1}. Scaling up from the central and northern MER (~400 km) to the Eastern Rift (~3,000 km), we might expect the Eastern Rift to produce ~3.9–32.7 Mt yr^{-1}. While the top of this estimate range is the same order of magnitude as the previous estimate (71 ± 33 Mt yr^{-1}) from Lee et al. (2016), it suggests that the diffuse CO_2 flux per length of rift from the central and northern MER is lower than that from the Magadi and Natron basins (1.3–10.9 kt yr^{-1} km^{-1} compared to 11.7–32.3 kt yr^{-1} km^{-1}). This may reflect differences in degassing behavior, for example in spatial frequency, size or type (edifice or off-edifice) of high-flux areas, between the MER and KRV.

Our data suggest that CO_2 degassing varies substantially along the Eastern Rift and reenforces that more surveys will be required to further constrain rift-scale emissions. With more data, more sophisticated statistical techniques could be applied to this problem (e.g., Bayesian approaches: De Angelis et al., 2014). Further profiles across degassing faults could be used to build models of CO_2 flux with distance from fault traces, given fault parameters such as throw and age. Identifying the abundance and distribution of faults concentrating CO_2 degassing remains a central obstacle in constraining rift-scale emissions.

Table 4
Estimating the Total CO_2 Flux From the Main Ethiopian Rift

Type	Flux per site (kt yr^{-1})	Number of sites	Total flux (kt yr^{-1})
On-edifice degassing	90–180 Aluto; Hutchison et al. (2015)	6 ± 1[a]	450–1,260
Off-edifice degassing	5–155 Habilo; this study	17 ± 3[b]	70–3,100
Total			520–4,360

[a]Fentale, Boset, Tulu Moye, Aluto, Corbetti, Oa/Shalla? Kone?
[b]Chokore, Bilate, Bodicho, Wondo Genet, Graha Quhe, Doredimtu, Butajira, Hippo Pool/Gargadi, Boku, Sodere Springs, Filoa, Hubicha, Habilo, Kessem River, Data volcano? Ashire volcano? Lake Chitu? Debre Tseyon? Gecha island? Western Fentale? (Figure 6 and supporting information Table 2).

4.3.2. Sources of CO_2 Emissions

The sources and modes of transport of magma and CO_2 in a rift are summarized in Figure 2. The flux of magma into the lithosphere is largely unknown and may be affected by multiple intrusions and melt pooling. As an instructive exercise the minimum crustal magma flux into a rift assuming that extension is accommodated exclusively through dike intrusion ("magmatic extension" hereafter; Agostini et al., 2011; Ebinger & Casey, 2001; Keir et al., 2006; Keranen et al., 2004) can be estimated from the extension rate and crustal thickness. For given values of initial CO_2 content, and assuming complete degassing of intruded magma, CO_2 emissions can be estimated.

The extension rate along the EARS varies from 0.7 to 5.2 mm yr^{-1} from the south to the north (Saria et al., 2014). Highest rates are located in Afar and along the MER (4.7–5.2 mm yr^{-1}). South of Lake Turkana the EARS splits into the magma-rich Eastern Rift and magma-poor Western Rift with extension rates varying north-south from 3.1 to 0.9 and 1.1 to

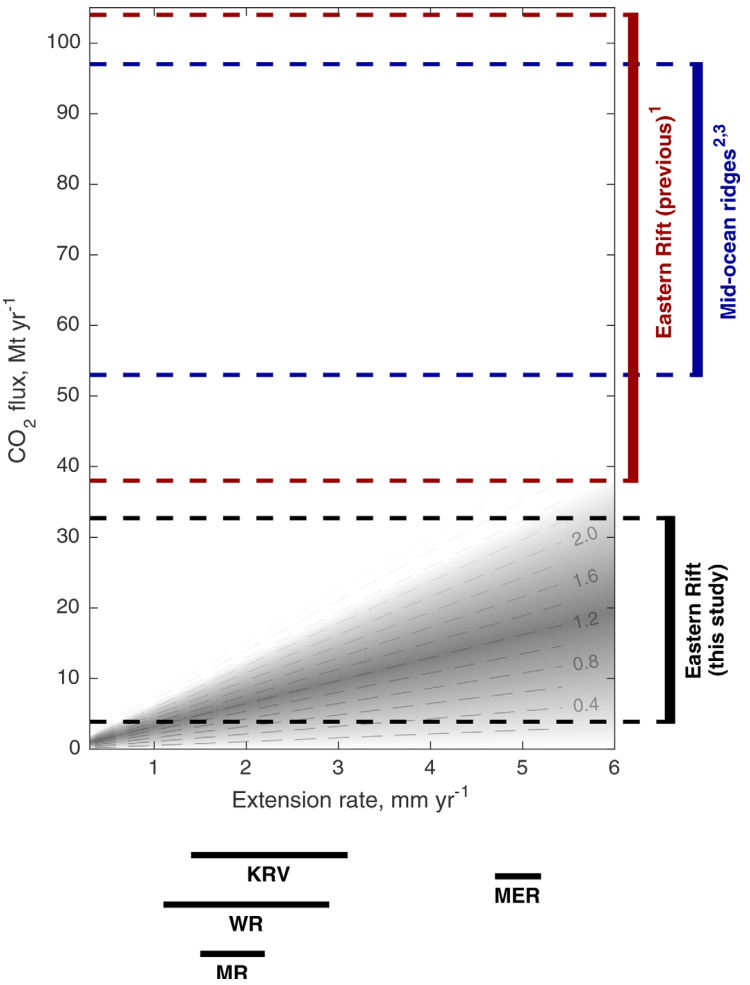

Figure 11. Estimating total CO_2 flux from magmatic extension of the Eastern Rift for a range of extension rates and initial carbon contents in magma (dashed lines show contours of equal initial carbon concentration in wt % in the range 0.02–2.4 wt %, Le Voyer et al., 2017). For comparison, estimated CO_2 flux from mid-ocean ridges (53–97 Mt yr^{-1}) is shown along with the existing estimate for the Eastern Rift (38–104 Mt yr^{-1}) and the Eastern Rift estimate from this study (3.9–32.7 Mt yr^{-1}). Complete degassing of highly enriched melt and intrusion of magma required to accommodate $\leq$ 5 mm yr^{-1} extension accounts for $\leq$32 Mt yr^{-1} CO_2 flux. Results assume magmatic extension along the 3,000 km Eastern Rift over a crustal thickness of 30 km, with an approximate magma density of 3,000 kg m^{-3}. Extension rates from Saria et al. (2014) shown by horizontal bars (MER, Main Ethiopian Rift; KRV, Kenyan Rift Valley; MR, Malawi Rift; and WR, Western Rift). References: [1]Lee et al. (2016), [2]Marty and Tolstikhin (1998), and [3]Kagoshima et al. (2015).

2.9 mm yr^{-1}, respectively. We consider the case that the Eastern Rift (MER and KRV, ~3,000 km) is entirely accommodated by magmatic intrusion. For an average crustal thickness of ~30 km and a fast extension rate of ~5 mm yr^{-1}, approximately 0.45 km^3 yr^{-1} of magma is required to accommodate crustal extension in the Eastern Rift.

Initial carbon contents in primary magmas may vary considerably (Helo et al., 2011; Le Voyer et al., 2017). The CO_2 concentration in melt inclusions provides a lower limit to the initial melt content, but a substantial proportion of CO_2 may be lost prior to melt inclusion formation. This shortcoming may be addressed by using ratios of CO_2 to a trace element on the basis of their similarly incompatible behavior during melting (most commonly Nd; Saal et al., 2002). Le Voyer et al. (2017) use CO_2 ratios and trace element compositions from the literature to provide a global range of upper mantle CO_2 content of 20–1,200 ppm, spanning the published estimates from many previous studies on depleted and enriched sources (e.g., Barry et al., 2014; Cartigny et al., 2008; Chavrit et al., 2014; Helo et al., 2011). Assuming an average melt fraction of 5–10%, this implies an initial CO_2 content of the melt before intrusion of 0.02–2.4 wt %.

Estimates of total emissions from magmatic extension for a range of initial CO_2 contents and extensions rates are shown in Figure 11. A maximum CO_2 concentration of 2.4 wt %, assuming total degassing of intruded magma, suggests that magmatic extension in the Eastern Rift contributes a maximum flux of ~32 Mt yr^{-1}, with lower initial CO_2 contents suggesting a contribution of approximately 6–18 Mt yr^{-1}. Our new estimate of 3.9–32.7 Mt yr^{-1} (section 4.3.1) is broadly consistent with degassing of a volume of magma equivalent to that accommodating extension.

This analysis is not intended to imply that extension related magmatism is the only possible source of deep CO_2 to the EAR. The flux of magma into the crust may exceed that accommodated by magmatic extension alone. Sills are observed in many volcanic rifted margins (Magee et al., 2016) and magma or mush reservoirs are inferred along the rift (e.g., Biggs et al., 2011; Desissa et al., 2013; Johnson et al., 2016; Roecker et al., 2017); these may represent additional sources of magmatic CO_2. Melting of easily fusible metasomes in the subcontinental lithospheric mantle (SCLM) has been posited as a key process in melt generation and strain localization within rifts (e.g., Rooney et al., 2014, 2017). Recent studies suggest abundant refertilization of the SCLM in southern and central Ethiopia by carbonate-rich, hydrous metasomatic agents (Casagli et al., 2017; Rooney et al., 2017; Trestrail et al., 2017). Carbon stored in metasomatized mantle could represent a significant additional source for CO_2 degassing. Similarly, decarbonation of crustal material (e.g., limestone) could contribute to the CO_2 flux (e.g., Parks et al., 2013; Sano & Marty, 1995). In fact, analysis of thermal springs in the Magadi and Natron basins suggests that a large proportion of dissolved CO_2 could be derived from a limestone end-member (up to 90.9% for individual samples; Lee et al., 2017).

In addition to CO_2 carried and/or released by magma intruded into the crust, CO_2 may also be supplied from deeper sources, including magmas intruded into, and pooled within, the lithosphere (Plasman et al., 2017). The sizes of these reservoirs are unknown. Earthquakes have been observed in the lower crust of the MER and KRV, interpreted as driven by fluids (Albaric et al., 2014; Keir et al., 2009). Through-going faults are hypothesized to concentrate CO_2 flow directly from the lithosphere (Lee et al., 2016), but the decreased

permeability due to lithostatic pressure at these depths may prohibit significant fluid flow (Manning & Ingebritsen, 1999). The behavior of faults and their permeability, and the behavior of CO_2-rich fluids, at lower crustal depths is poorly constrained and further experimental studies would be valuable.

These additional sources of CO_2 may also vary along the Eastern Rift and constraining the provenance of diffuse CO_2 is challenging. As previously discussed (section 1), the mantle carbon flux out of the Eastern Rift inferred from the Magadi and Natron basins (Lee et al., 2016) may be an overestimate depending on how representative these basins are, the scaling methodologies employed, and the interpretation of isotopic analysis. Lee et al. (2016) interpret the carbon-isotopic compositions of soil gases to suggest a dominantly mantle contribution to the observed CO_2 flux in the KRV. However, there is uncertainty in assigning a provenance to soil gases, due to overlapping $\delta^{13}C$ compositions between air (–8‰) and mantle-derived gases (–3 to −8‰). The soil gas collected for isotopic analysis included an unquantified contribution from the air, complicated by the addition of isotopically light biogenic carbon, which reduced the isotopic value of some samples to significantly below the mantle-air mixing line (–11.7‰). Lee et al. (2016) account for this uncertainty by supposing an average mantle contribution of 10%, however the true value may be lower. The CO_2 concentrations in the Lee et al. (2016) measurements ranged from 500 to 2,000 ppm, and can be used alongside isotopic ratios to estimate the relative proportions of the air and mantle sources in the samples. For example, if we take 400 ppm and 11.9 wt % as the CO_2 concentration in air and mantle-derived gases respectively (Fischer & Chiodini, 2015), not accounting for biogenic input, we find a mantle contribution of just 1%. Air contamination is therefore difficult to account for accurately and could be substantial. A proportion of the diffuse CO_2 flux in this region could also be due to heating and fracturing of carbonate rocks, which would provide a similar isotopic signature to mantle (Lee et al., 2017).

If the high estimates for deep CO_2 flux in these areas are real, they may represent a large proportion of the total Eastern Rift contribution, in which case scaling up from these regions would overestimate the total flux. Understanding the factors controlling the spatial variability of rift CO_2 emissions must remain a research priority. The time dependence of CO_2 emissions from rift sites also remains unknown, and repeated measurements to provide a temporal dimension to our understanding of diffuse CO_2 degassing remains a key research priority.

In summary, our new estimate suggests that, although CO_2 emissions from the Eastern Rift of the EARS are likely lower than emissions from the global mid-ocean ridge system, they are still substantial. The mechanisms resulting in such large fluxes are likely to be significant for our understanding of rift dynamics, relating volatile movement and melt generation to lithospheric deformation.

5. Conclusions

Understanding diffuse CO_2 degassing in volcanically active areas is important in terms of global CO_2 budgets and hazards. A series of diffuse soil surveys in the Main Ethiopian Rift (MER) have shown that CO_2 flux varies greatly on three spatial scales: within concentrated zones of emission, between faults in the same basin and between adjacent terrains. CO_2 degassing is not merely restricted to volcanic edifices, however off-edifice degassing is not distributed evenly along the MER. The areas of Butajira and Habilo emit a significant flux of CO_2, suggesting magma storage some lateral distance from the nearest volcanic center. The patchiness of degassing presents difficulties in scaling up to estimations of rift-related diffuse CO_2 emissions. A compilation of hot spring and fumarole locations elucidates the distribution of geothermal areas along the rift; numerous, small sites of activity are found, similar to Habilo and Butajira.

Extrapolation from our surveys using the distribution of geothermal areas suggests a total CO_2 flux from the Main Ethiopian Rift of 0.52–4.36 Mt yr^{-1}. In the case that the MER is representative of the entire Eastern Rift, we predict a flux of 3.9–32.7 Mt yr^{-1} over this region. Although the maximum and minimum of the ranges are consistent, this result is significantly lower than the total CO_2 flux estimated by extrapolation from the Kenya Rift Valley (38–104 Mt yr^{-1}), possibly implying a fundamental difference in the deep carbon cycle between the two areas of the rift. Additional surveys along the Eastern Rift are required to further test these extrapolated estimates, given the uncertainty over how representative either test case is for the Eastern Rift as a whole.

The results of this study suggest that, while diffuse degassing of deep CO_2 within continental rifts is a large contributor to the long-term global carbon budget, its total flux may have been previously overestimated. Nevertheless, the magnitude of emissions raises questions over the CO_2 sources and mechanisms associated with rifting. We estimate that a range of 6–18 Mt yr^{-1} (with an absolute maximum of 32 Mt yr^{-1}) CO_2 along the Eastern Rift can be accounted for by magmatic intrusion into the crust as it accommodates extension. Additional magmatic intrusions in the form of sills and magma mush zones in addition to melting a lithosphere enriched in volatiles and assimilation of crustal material may play an important role. Further work toward estimating total magma flux into rifts is required.

The release of deep CO_2 through large faults has been posited as a mechanism for transporting high fluxes through the lithosphere. Investigation into the permeability structures as well as the decoupling of CO_2-rich fluid and melt at lower crustal depths are valuable next steps. The high flux of volatiles through the East African Rift System has important implications for rift development, the global carbon cycle and regimes of magma storage within the lithosphere and crust.

Acknowledgments
This work was supported by a studentship from NERC as part of the Environmental Research DTP (University of Oxford). Many thanks to K. Whaler, J. Hübert, D. Keir, and the Institute of Geophysics, Space Science and Astronomy (IGSSA) at Addis Ababa University for help in the field. The Habilo campaign was coled by T. Elliott and M. Sharp from Hotspur Geothermal, whom we thank for fieldwork, logistical support, and background information. We thank Seifu Kebede from the University of Addis Ababa who provided data on locations for hot springs along the Main Ethiopian Rift. This work is a contribution to the Natural Environment Research Council funded RiftVolc project (NE/L013932/1, Rift volcanism: past, present, and future). T.A.M. and D.M.P. are supported by and contribute to the NERC Centre for the Observation and Modelling of Earthquakes, Volcanoes, and Tectonics (COMET). Will Hutchison and Dave Hilton are thanked for useful discussions. The data used in this paper are listed in the references, tables, and supporting information. The authors thank Tobias Fischer, an anonymous reviewer and the Editor, for helpful comments that improved the manuscript.

References

Abebe, B., Acocella, V., Korme, T., & Ayalew, D. (2007). Quaternary faulting and volcanism in the Main Ethiopian Rift. *Journal of African Earth Sciences*, *48*(2–3), 115–124. https://doi.org/10.1016/j.jafrearsci.2006.10.005

Abera, F., Dander, K., Mengste, A., Burusa, G., & Beyene, T. (2014). *Magnetic and gravity survey of gedemsa geothermal prospect area-Main Ethiopian Rift*, Paper presented at ARGEO-C5 Conference, Arusha, Tanzania, October 29–31, 2014.

Abiye, T. A., & Haile, T. (2008). Geophysical exploration of the Boku geothermal area, Central Ethiopian Rift. *Geothermics*, *37*(6), 586–596. https://doi.org/10.1016/j.geothermics.2008.06.004

Agostini, A., Bonini, M., Corti, G., Sani, F., & Mazzarini, F. (2011). Fault architecture in the Main Ethiopian Rift and comparison with experimental models: Implications for rift evolution and Nubia-Somalia kinematics. *Earth and Planetary Science Letters*, *301*(3–4), 479–492. https://doi.org/10.1016/j.epsl.2010.11.024

Albaric, J., Déverchère, J., Perrot, J., Jakovlev, A., & Deschamps, A. (2014). Deep crustal earthquakes in North Tanzania, East Africa: Interplay between tectonic and magmatic processes in an incipient rift. *Geochemistry, Geophysics, Geosystems*, *15*, 374–394. https://doi.org/10.1002/2013GC005027

Allard, P., Jean-Baptiste, P., Alessandro, W. D., Pare, F., Parisi, B., & Flehoc, C. (1997). Mantle-derived helium and carbon in groundwaters and gases of Mount Etna, Italy. *Earth and Planetary Science Letters*, *148*(97), 501–516.

Alula, D., Boccaletti, M., Getaneh, A., Mazzuoli, R., Tortorici, L., & Trua, T. (1992). *Geological map of the Nazret-Dera Region (Main Ethiopian Rift)* (scale 1:50 000). Consiglio Nazionale delle Ricerche, Rome, Italy.

Ayele, A., Teklemariam, M., & Kebede, S. (2002). *Geothermal resource exploration in the Abaya and Tulu Moye-Gedemsa Geothermal Prospects, Main Ethiopian Rift* (internal report, 172 pp.). Addis Ababa, Ethiopia: Geological Survey of Ethiopia.

Ayenew, T., Kebede, S., & Alemyahu, T. (2008). Environmental isotopes and hydrochemical study applied to surface water and groundwater interaction in the Awash River basin. *Hydrological Processes*, *22*, 1548–1563. https://doi.org/10.1002/hyp.6716

Bahiru, E. A. (2007). *Structural study and its effect on thermal activities of Tulu Moye- Gedemsa Area* (MSc thesis, 88 pp.). Addis Ababa, Ethiopia: Addis Ababa University.

Barry, P. H., Hilton, D. R., Fischer, T. P., De Moor, J. M., Mangasini, F., & Ramirez, C. (2013). Helium and carbon isotope systematics of cold "mazuku" CO_2 vents and hydrothermal gases and fluids from Rungwe Volcanic Province, southern Tanzania. *Chemical Geology*, *339*, 141–156. https://doi.org/10.1016/j.chemgeo.2012.07.003

Barry, P. H., Hilton, D. R., Füri, E., Halldórsson, S. A., & Grönvold, K. (2014). Carbon isotope and abundance systematics of Icelandic geothermal gases, fluids and subglacial basalts with implications for mantle plume-related CO_2 fluxes. *Geochimica et Cosmochimica Acta*, *134*, 74–99. https://doi.org/10.1016/j.gca.2014.02.038

Bastow, I. D., Stuart, G. W., Kendall, J.-M., & Ebinger, C. J. (2005). Upper-mantle seismic structure in a region of incipient continental breakup: northern Ethiopian rift. *Geophysical Journal International*, *162*, 479–493. https://doi.org/10.1111/j.1365-246X.2005.02666.x

Bastow, I. D., Nyblade, A. A., Stuart, G. W., Rooney, T. O., & Benoit, M. H. (2008), Upper mantle seismic structure beneath the Ethiopian hot spot: Rifting at the edge of the African low-velocity anomaly. *Geochemistry, Geophysics, Geosystems*, *9*(12), 1–25. https://doi.org/10.1029/2008GC002107

Bekele, B., Mamo, T., Teclu, A., & Kebede, Y. (2007). *Compilation of the geoscientific study of the Dofan-Fantale Geothermal Prospect, Ethiopia* (internal report, 140 pp.). Addis Ababa, Ethiopia: Geological Survey of Ethiopia.

Berner, R. A., Lasaga, A. C., & Garrels, R. M. (1983). The carbonate-silicate geochemical cycle and its effect on atmospheric carbon dioxide over the past 100 million years. *American Journal of Science*, *283*(7), 641–683. https://doi.org/10.2475/ajs.283.7.641

Beyene, K. (2000). *Preliminary geochemical report on Tulumoye-Gedemsa and the surrounding areas* (internal report, 8 pp.). Addis Ababa, Ethiopia: Geological Survey of Ethiopia.

Biggs, J., Amelung, F., Gourmelen, N., Dixon, T. H., & Kim, S. W. (2009). InSAR observations of 2007 Tanzania rifting episode reveal mixed fault and dyke extension in an immature continental rift. *Geophysical Journal International*, *179*(1), 549–558. https://doi.org/10.1111/j.1365-246X.2009.04262.x

Biggs, J., Bastow, I. D., Keir, D., & Lewi, E. (2011). Pulses of deformation reveal frequently recurring shallow magmatic activity beneath the Main Ethiopian Rift. *Geochemistry, Geophysics, Geosystems*, *12*, Q0AB10. https://doi.org/10.1029/2011GC003662

Braddock, M., Biggs, J., Watson, I. M., Hutchison, W., Pyle, D. M., & Mather, T. A. (2017). Satellite observations of fumarole activity at Aluto volcano, Ethiopia: Implications for geothermal monitoring and volcanic hazard. *Journal of Volcanology and Geothermal Research*, *341*, 70–83. https://doi.org/10.1016/j.jvolgeores.2017.05.006

Buck, W. R. (2004). Consequences of asthenospheric variability on continental rifting. In *Rheology and deformation of the lithosphere at continental margins* (pp. 1–30). New York: Columbia University Press.

Burton, M. R., Sawyer, G. M., & Granieri, D. (2013). Deep carbon emissions from volcanoes. *Reviews in Mineralogy and Geochemistry*, *75*(1), 323–354. https://doi.org/10.2138/rmg.2013.75.11

Camarda, M., De Gregorgio, S., Di Martino, R. M. R., & Favara, R. (2016). Temporal and spatial correlations between soil CO_2 flux and crustal stress. *Journal of Geophysical Research: Solid Earth*, *121*, 7071–7085. https://doi.org/10.1002/2016JB01329

Cardellini, C., Chiodini, G., & Frondini, F. (2003). Application of stochastic simulation to CO_2 flux from soil: Mapping and quantification of gas release. *Journal of Geophysical Research*, *108*(B9), 2425. https://doi.org/10.1029/2002JB002165

Cartigny, P., Pineau, F., Aubaud, C., & Javoy, M. (2008). Towards a consistent mantle carbon flux estimate: Insights from volatile systematics (H_2O/Ce, δD, CO_2/Nb) in the North Atlantic mantle (14°N and 34°N). *Earth and Planetary Science Letters*, *265*(3–4), 672–685. https://doi.org/10.1016/j.epsl.2007.11.011

Casagli, A., Frezzotti, M. L., Peccerill, A., Tiepolo, M., & Astis, D. (2017). (Garnet)-spinel peridotite xenoliths from Mega (Ethiopia): Evidence for rejuvenation and dynamic thinning of the lithosphere beneath the southern Main Ethiopian Rift. *Chemical Geology*, *455*, 231–248. https://doi.org/10.1016/j.chemgeo.2016.11.001

Chavrit, D., Humler, E., & Grasset, O. (2014). Mapping modern CO_2 fluxes and mantle carbon content all along the mid-ocean ridge system. *Earth and Planetary Science Letters*, *387*, 229–239. https://doi.org/10.1016/j.epsl.2013.11.036

Chiodini, G., Baldini, A., Barberi, F., Carapezza, M. L., Cardellini, C., Frondini, F., . . . Ranaldi, M. (2007). Carbon dioxide degassing at Latera caldera (Italy): Evidence of geothermal reservoir and evaluation of its potential energy. *Journal of Geophysical Research*, *112*, B12204. https://doi.org/10.1029/2006JB004896

Chiodini, G., Caliro, S., Cardellini, C., Avino, R., Granieri, D., & Schmidt, A. (2008). Carbon isotopic composition of soil CO_2 efflux, a powerful method to discriminate different sources feeding soil CO_2 degassing in volcanic-hydrothermal areas. *Earth and Planetary Science Letters*, *274*(3–4), 372–379. https://doi.org/10.1016/j.epsl.2008.07.051

Chiodini, G., Cardellini, C., Amato, A., Boschi, E., Caliro, S., Frondini, F., & Ventura, G. (2004). Carbon dioxide Earth degassing and seismogenesis in central and southern Italy. *Geophysical Research Letters*, *31*, L07615. https://doi.org/10.1029/2004GL019480

Chiodini, G., Cioni, R., Guidi, M., Raco, B., & Marini, L. (1998). Soil CO_2 flux measurements in volcanic and geothermal areas. *Applied Geochemistry*, *13*(5), 543–552. https://doi.org/10.1016/S0883-2927(97)00076-0

Chiodini, G., & Frondini, F. (2001). Carbon dioxide degassing from the Albani Hills volcanic region, Central Italy. *Chemical Geology*, *177*(1), 67–83. https://doi.org/10.1016/S0009-2541(00)00382-X

Chiodini, G., Frondini, F., Cardellini, C., Granieri, D., Marini, L., & Ventura, G. (2001). CO_2 degassing and energy release at Solfatara volcano, Campi Flegrei, Italy. *Journal of Geophysical Research*, *106*(B8), 16213–16221.

Chiodini, G., Frondini, F., Kerrick, D. M., Rogie, J., Parello, F., Peruzzi, L., & Zanzari, A. R. (1999). Quantification of deep CO_2 fluxes from Central Italy. Examples of carbon balance for regional aquifers and of soil diffuse degassing. *Chemical Geology*, *159*(1), 205–222. https://doi.org/10.1016/S0009-2541(99)00030-3

Chiodini, G., Granieri, D., Avino, R., Caliro, S., Costa, A., Minopoli, C., & Vilardo, G. (2010). Non-volcanic CO_2 Earth degassing: Case of Mefite d'Ansanto (southern Apennines), Italy. *Geophysical Research Letters*, *37*, L11303. https://doi.org/10.1029/2010GL042858

D'Alessandro, W., Giammanco, S., Parello, F., & Valenza, M. (1997). CO_2 output and $\delta^{13}C(CO_2)$ from Mount Etna as indicators of degassing of shallow asthenosphere. *Bulletin of Volcanology*, *58*(6), 455–458. https://doi.org/10.1007/s004450050154

Darling, W. G., Gizaw, B., & Arusei, M. K. (1996). Lake-groundwater relationships and fluid-rock interaction in the East African Rift Valley: Isotopic evidence. *Journal of African Earth Sciences*, *22*(4), 423–431. https://doi.org/10.1016/0899-5362(96)00026-7

Dasgupta, R. (2013). Ingassing, storage, and outgassing of terrestrial carbon through geologic time. *Reviews in Mineralogy and Geochemistry*, *75*, 183–229. https://doi.org/10.2138/rmg.2013.75.7

Dawson, J. B., Pyle, D. M., & Pinkerton, H. (1996). Evolution of natrocarbonatite from a wollastonite nephelenite parent: Evidence from the June 1993 eruption of Oldoinyo Lengai, Tanzania. *Journal of Geology*, *104*, 41–54.

De Angelis, D., Presanis, A. M., Conti, S., & Ades, A. E. (2014). Estimation of HIV burden through Bayesian evidence synthesis. *Statistical Science*, *29*, 9–17. https://doi.org/10.1214/13-STS428

de Moor, J. M., Fischer, T. P., Sharp, Z. D., Hilton, D. R., Barry, P. H., Mangasini, F., & Ramirez, C. (2013). Gas chemistry and nitrogen isotope compositions of cold mantle gases from Rungwe Volcanic Province, southern Tanzania. *Chemical Geology*, *339*, 30–42. https://doi.org/10.1016/j.chemgeo.2012.08.004

Desissa, M., Johnson, N. E., Whaler, K. A., Hautot, S., Fisseha, S., & Dawes G. J. K. (2013). A mantle magma reservoir beneath an incipient mid-ocean ridge in Afar, Ethiopia. *Nature Geoscience*, *6*(10), 861. http://dx.doi.org/10.1038/ngeo1925

Di Paola, G. M. (1970). *Geological-geothermal report on the central part of the Ethiopian Rift Valley* (internal report). Addis Ababa, Ethiopia: Ministry of Mines.

Dockrill, B., & Shipton, Z. K. (2010). Structural controls on leakage from a natural CO_2 geologic storage site: Central Utah, U.S.A. *Journal of Structural Geology*, *32*(11), 1768–1782. https://doi.org/10.1016/j.jsg.2010.01.007

Ebinger, C. J., & Casey, M. (2001). Continental breakup in magmatic provinces: An Ethiopian example. *Geology*, *29*(6), 527–530. http://www.bls.gov/cex/https://doi.org/10.1130/0091-7613(2001)029<0527:CBIMPA>2.0.CO;2

Ebinger, C. (2005). Continental break-up: The East African perspective. *Astronomy & Geophysics*, *46*(2), 2–16.

Etiope, G., Beneduce, P., Calcara, M., Favali, P., Frugoni, F., Schiattarella, M., & Smriglio, G. (1999). Structural pattern and CO_2–CH_4 degassing of Ustica Island, Southern Tyrrhenian basin. *Journal of Volcanology and Geothermal Research*, *88*(4), 291–304. https://doi.org/10.1016/S0377-0273(99)00010-4

Etiope, G., & Martinelli, G. (2002). Migration of carrier and trace gases in the geosphere: An overview. *Physics of the Earth and Planetary Interiors*, *129*(3–4), 185–204. https://doi.org/10.1016/S0031-9201(01)00292-8

Evans, W. C., Bergfeld, D., McGimsey, R. G., & Hunt, A. G. (2009). Diffuse gas emissions at the Ukinrek Maars, Alaska: Implications for magmatic degassing and volcanic monitoring. *Applied Geochemistry*, *24*(4), 527–535. https://doi.org/10.1016/j.apgeochem.2008.12.007

Faulkner, D. R., Jackson, C. A. L., Lunn, R. J., Schlische, R. W., Shipton, Z. K., Wibberley, C. A. J., & Withjack, M. O. (2010). A review of recent developments concerning the structure, mechanics and fluid flow properties of fault zones. *Journal of Structural Geology*, *32*(11), 1557–1575. https://doi.org/10.1016/j.jsg.2010.06.009

Favara, R., Giammanco, S., Inguaggiato, S., & Pecoraino, G. (2001). Preliminary estimate of CO_2 output from Pantelleria Island volcano (Sicily, Italy): Evidence of active mantle degassing. *Applied Geochemistry*, *16*(7), 883–894. https://doi.org/10.1016/S0883-2927(00)00055-X

Ferguson, D. J., Maclennan, J., Bastow, I. D., Pyle, D. M., Jones, S. M., Keir, D., . . . Yirgu, G. (2013). Melting during late stage rifting in Afar is hot and deep. *Nature*, *499*, 70–73.

Fischer, T. P., Burnard, P., Marty, B., Hilton, D. R., Füri, E., Palhol, F., . . . Mangasini, F. (2009). Upper-mantle volatile chemistry at Oldoinyo Lengai volcano and the origin of carbonatites. *Nature*, *459*(7243), 77–80. https://doi.org/10.1038/nature07977

Fischer, T. P., & Chiodini, G. (2015). Volcanic, magmatic and hydrothermal gases. In H. Sigurdsson, B. Houghton, S. R. McNutt, H. Rymer, & J. Stix (Eds.), *The encyclopedia of volcanoes* (pp. 779–798). New York, NY: Academic Press.

Gallacher, R. J., Keir, D., Harmon, N., Stuart, G., Leroy, S., Hammond, J. O. S., . . . Ahmed, A. (2016). The initiation of segmented buoyancy-driven melting during continental breakup. *Nature Communications*, *7*, 13110. https://doi.org/10.1038/ncomms13110

Geological Survey of Ethiopia and United Nations. (1976). *Geological maps of Fike (0738 A4), Zeway (0738 B1), Chefe Jila (0738 B2), Kersa (0738 B4), Sembete (0738 C2), and Negele Arusi (0738 D1)* (scale 1:50,000). Addis Ababa, Ethiopia.

Giammanco, S., Parello, F., Gambardella, B., Schifano, R., Pizzullo, S., & Galante, G. (2007). Focused and diffuse effluxes of CO_2 from mud volcanoes and mofettes south of Mt. Etna (Italy). *Journal of Volcanology and Geothermal Research*, *165*(1), 46–63. https://doi.org/10.1016/j.jvolgeores.2007.04.010

Gibson, I. L. (1974). A review of the geology, petrology and geochemistry of the Volcano Fantale. *Bulletin of Volcanology*, *38*(2), 791–802. https://doi.org/10.1007/BF02596908

Gíslason, G., Eysteinsson, H., Björnsson, G., & Harðardóttir, V. (2015). Results of surface exploration in the Corbetti Geothermal Area, Ethiopia. Paper presented at *World Geothermal Congress*, Melbourne, Australia, 19-25 April 2015.

Gizaw, B. (1996). The origin of high bicarbonate and fluoride concentrations in waters of the Main Ethiopian Rift Valley, East African Rift system. *Journal of African Earth Sciences*, *22*(4), 391–402. https://doi.org/10.1016/0899-5362(96)00029-2

Haile Selassie, D. (1984). *Compiled report on low enthalpy geothermal resources of Ethiopia* (internal report, 48 pp.). Addis Ababa, Ethiopia: Ministry of Mines and Energy.

Helo, C., Longpré, M.-A., Shimizu, N., Clague, D. A., & Stix, J. (2011). Explosive eruptions at mid-ocean ridges driven by CO_2-rich magmas. *Nature Geoscience*, *4*(4), 260–263. https://doi.org/10.1038/ngeo1104

Hernández, P. A., Pérez, N. M., Fridriksson, T., Egbert, J., Ilyinskaya, E., Thárhallsson, A., . . . Notsu, K. (2012). Diffuse volcanic degassing and thermal energy release from Hengill volcanic system, Iceland. *Bulletin of Volcanology*, *74*(10), 2435–2448. https://doi.org/10.1007/s00445-012-0673-2

Hernández Perez, P., Notsu, K., Tsurumi, M., More, T., Ohno, M., Shimoike, Y., . . . Perez, N. (2003). Carbon dioxide emissions from soils at Hakkoda, north Japan. *Journal of Geophysical Research*, *108*(B4), 2210. https://doi.org/10.1029/2002JB001847

Hochstein, M. P., Oluma, B., & Hole, H. (2017). Early exploration of the Aluto geothermal field, Ethiopia (History of discovery well LA-3). *Geothermics*, *66*, 73–84. https://doi.org/10.1016/j.geothermics.2016.11.010

Hudgins, T. R., Mukasa, S. B., Simon, A. C., Moore, G. & Barifaijo, E. (2015). Melt inclusion evidence for CO2-rich melts beneath the western branch of the East African Rift: implications for long-term storage of volatiles in the deep lithospheric mantle *Contributions to Mineralogy and Petrology*, *169*(5), 1–18. https://doi.org/10.1007/s00410-015-1140-9

Hutchison, W., Biggs, J., Mather, T. A., Pyle, D. M., Lewi, E., Yirgu, G., . . . Tobias, P. (2016a). Causes of unrest at silicic calderas in the East African Rift: New constraints from InSAR and soil-gas chemistry at Aluto volcano, Ethiopia. *Geochemistry, Geophysics, Geosystems*, *17*, 3008–3030. https://doi.org/10.1002/2016GC006395

Hutchison, W., Fusillo, R., Pyle, D. M., Mather, T. A., Blundy, J. D., Biggs, J., . . . Calvert, A. T. (2016b). A pulse of mid-Pleistocene rift volcanism in Ethiopia at the dawn of modern humans. *Nature Communications*, *7*, 13192. https://doi.org/10.1038/ncomms13192

Hutchison, W., Mather, T. A., Pyle, D. M., Biggs, J., & Yirgu, G. (2015). Structural controls on fluid pathways in an active rift system: A case study of the Aluto volcanic complex. *Geosphere*, *11*(3), 542–562. https://doi.org/10.1130/GES01119.1

Ibs-von Seht, M., Blumenstein, S., Wagner, R., Hollnack, D., & Wohlenberg, J. (2001). Seismicity, seismotectonics and crustal structure of the southern Kenya Rift—New data from the Lake Magadi area. *Geophysical Journal International*, *146*, 439–453. https://doi.org/10.1046/j.0956-540x.2001.01464.x

Italiano, F., Martelli, M., Martinelli, G., & Nuccio, P. M. (2000). Geochemical evidence of melt intrusions along lithospheric faults of the Southern Apennines, Italy' Geodynamic and seismogenic implications. *Journal of Geophysical Research*, *105*(B6), 13569–13578. https://doi.org/10.1029/2000JB900047

Johnson, N. E., Whaler, K. A., Hautot, S., Fisseha, S., Desissa, M., & Dawes, G. J. K. (2016). Magma imaged magnetotellurically beneath an active and an inactive magmatic segment in Afar, Ethiopia. *Geological Society, London, Special Publications*, *420*(1), 105–125. https://doi.org/10.1144/SP420.11

Kagoshima, T., Sano, Y., Takahata, N., Maruoka, T., Fischer, T. P., & Hattori, K. (2015). Sulphur geodynamic cycle. *Scientific Reports*, *5*, 8330. https://doi.org/10.1038/srep08330

Kebede, S. (2012). Geothermal exploration and development in Ethiopia: Status and future plan. Paper presented at *Exploration for Geothermal Resources, Short Course VII*, Lake Bogoria and Lake Naivasha, Kenya.

Kebede, S., Mamo, T., & Abebe, T. (1985). *Geological report and explanation to the geological map of Aluto-Langano geothermal area: Addis Ababa* (60 pp.). Addis Ababa, Ethiopia: Ethiopian Institute of Geological Surveys.

Keir, D., Bastow, I. D., Corti, G., Mazzarini, F., & Rooney, T. O. (2015). The origin of along-rift variations in faulting and magmatism in the Ethiopian Rift. *Tectonics*, *34*(3), 464–477. https://doi/10.1002/2014TC003698

Keir, D., Ebinger, C. J., Stuart, G. W., Daly, E., & Ayele, A. (2006). Strain accommodation by magmatism and faulting as rifting proceeds to breakup: Seismicity of the Northern Ethiopian Rift. *Journal of Geophysical Research*, *111*, B05314. https://doi.org/10.1029/2005JB003748

Keir, D., Hamling, I. J., Ayele, A., Calais, E., Ebinger, C., Wright, T. J., . . . Bennati, L. (2009). Evidence for focused magmatic accretion at segment centers from lateral dike injections captured beneath the Red Sea Rift in Afar. *Geology*, *37*(1), 59–62. https://doi.org/10.1130/G25147A.1

Kelemen, P. B., & Manning, C. E. (2015). Reevaluating carbon fluxes in subduction zones, what goes down, mostly comes up. *Proceedings of the National Academy of Sciences of the United States of America*, *112*(30), 3997–4006. https://doi.org/10.1073/pnas.1507889112

Keranen, K., & Klemperer, S. L. (2008). Discontinuous and diachronous evolution of the Main Ethiopian Rift: Implications for development of continental rifts. *Earth and Planetary Science Letters*, *265*(1–2), 96–111. https://doi.org/10.1016/j.epsl.2007.09.038

Keranen, K., Klemperer, S. L., Gloaguen, R., & EAGLE Working Group. (2004). Three-dimensional seismic imaging of a protoridge axis in the Main Ethiopian rift. *Geology*, *32*(11), 949–952. https://doi.org/10.1130/G20737.1

Koepenick, K. W., Brantley, S. L., Thompson, J. M., Rowe, G. L., Nyblade, A. A., & Moshy, C. (1996). Volatile emissions from the crater and flank of Oldoinyo Lengai volcano, Tanzania. *Journal of Geophysical Research*, *101*(B6), 13819–13830. https://doi.org/10.1029/96JB00173

Le Voyer, M., Kelley, K. A., Cottrell, E., & Hauri, E. H. (2017). Heterogeneity in mantle carbon content from CO_2-undersaturated basalts. *Nature Communications*, *8*, 14062. https://doi.org/10.1038/ncomms14062

Lee, H., Fischer, T. P., Muirhead, J. D., Ebinger, C. J., Kattenhorn, S. A., Sharp, Z. D., . . . Sano, Y. (2017). Incipient rifting accompanied by the release of subcontinental lithospheric mantle volatiles in the Magadi and Natron basin, East Africa. *Journal of Volcanology and Geothermal Research*. https://doi.org/10.1016/j.jvolgeores.2017.03.017, in press.

Lee, H., Muirhead, J. D., Fischer, T. P., Ebinger, C. J., Kattenhorn, S. A., Sharp, Z. D., & Kianji, G. (2016). Massive and prolonged deep carbon emissions associated with continental rifting. *Nature Geoscience*, (January), 1–6. https://doi.org/10.1038/NGEO2622

Lucic, G., Stix, J., & Wing, B. (2015). Structural controls on the emission of magmatic carbon dioxide gas, Long Valley Caldera, USA. *Journal of Geophysical Research: Solid Earth*, *120*, 2262–2278. https://doi.org/10.1002/2014JB011760

Magee, C., Muirhead, J. D., Karvelas, A., Holford, S. P., Jackson, C. A. L., Bastow, I. D., . . . Shtukert, O. (2016). Lateral magma flow in mafic sill complexes. *Geosphere*, *12*(3), 809–841. https://doi.org/10.1130/GES01256.1

Manning, C. E., & Ingebritsen, S. E. (1999). Permeability of the continental crust: Implications of geothermal data and metamorphic systems. *Reviews of Geophysics*, *37*(1), 127–150.

Marty, B., & Tolstikhin, I. N. (1998). CO_2 fluxes from mid-ocean ridges, arcs and plumes. *Chemical Geology*, *145*(3–4), 233–248. https://doi.org/10.1016/S0009-2541(97)00145-9

Mengistu, Y. (2016). *Detection of geothermal anomalies using Landsat 8 thermal infrared data in Tulu Moye geothermal prospect, Main Ethiopia Rift* (MSc thesis, 98 pp.). Addis Ababa, Ethiopia: Addis Ababa University.

Ministry of Water Resources (MOWR). (2008). *Butajira–Ziway areas development study: Hydrogeology and grownd water modeling* (internal report, 102 pp.). Addis Ababa, Ethiopia: Ethiopian Water Technology Centre.

Mohr, P., Mitchell, J. G., & Raynolds, R. G. H. (1980). Quaternary volcanism and faulting at O'A Caldera, Central Ethiopian Rift. *Bulletin of Volcanology*, *43*(1), 173–189. https://doi.org/10.1007/BF02597619

Mörner, N.-A., & Etiope, G. (2002). Carbon degassing from the lithosphere. *Global and Planetary Change*, *33*(1), 185–203. https://doi.org/10.1016/S0921-8181(02)00070-X

Muirhead, J. D., Kattenhorn, S. A., Lee, H., Mana, S., Turrin, B. D., Fischer, T. P., . . . Stamps, D. S. (2016). Evolution of upper crustal faulting assisted by magmatic volatile release during early-stage continental rift development in the East African Rift. *Geosphere*, *12*(6), GES01375.1, https://doi.org/10.1130/GES01375.1

Oppenheimer, C., Burton, M. R., Durieux, J., & Pyle, D. M. (2002). Open-path Fourier transform spectroscopy of gas emissions from Oldoinyo Lengai volcano, Tanzania. *Optics and Lasers in Engineering*, *37*, 203–214.

Parks, M. M., Caliro, S., Chiodini, G., Pyle, D. M., Mather, T. A., Berlo, K., . . . Raptakis, C. (2013). Distinguishing contributions to diffuse CO_2 emissions in volcanic areas from magmatic degassing and thermal decarbonation using soil gas ^{222}Rn- δ^{13}C systematics: Application to Santorini volcano, Greece. *Earth and Planetary Science Letters*, *377–378*, 180–190. https://doi.org/10.1016/j.epsl.2013.06.046

Pérez, N. M., Hernández, P. A., Padilla, G., Nolasco, D., Barrancos, J., Melían, G., . . . Ibarra, M. (2011). Global CO_2 emission from volcanic lakes. *Geology*, *39*(3), 235–238. https://doi.org/10.1130/G31586.1

Plasman, M., Tiberi, C., Ebinger, C., Gautier, S., Albaric, J., Peyrat, S., . . . Gama, R. (2017). Lithospheric low-velocity zones associated with a magmatic segment of the Tanzanian Rift, East Africa. *Geophysical Journal International*, *210*, 465–481. https://doi.org/10.1093/gji/ggx177

Pürschel, M., Gloaguen, R., & Stadler, S. (2013). Geothermal activities in the Main Ethiopian Rift: Hydrogeochemical characterization of geothermal waters and geothermometry applications (Dofan-Fantale, Gergede-Sodere, Aluto-Langano). *Geothermics*, *47*, 1–12. https://doi.org/10.1016/j.geothermics.2013.01.001

Rampey, M. L., Oppenheimer, C., Pyle, D. M., & Yirgu, G. (2010). Caldera-forming eruptions of the Quaternary Kone Volcanic Complex, Ethiopia. *Journal of African Earth Sciences*, *58*(1), 51–66. https://doi.org/10.1016/j.jafrearsci.2010.01.008

Reyners, M., Eberhart-Phillips, D., & Stuart, G. (2007). The role of fluids in lower-crustal earthquakes near continental rifts. *Nature*, *446*, 1075–1078. https://doi.org/10.1038/nature05743

Robertson, E., Biggs, J., Edmonds, M., Clor, L., Fischer, T. P., Vye-Brown, C., . . . Kandie, R. (2016). Diffuse degassing at Longonot volcano, Kenya: Implications for CO_2 flux in continental rifts. *Journal of Volcanology and Geothermal Research*, *327*, 208–222. https://doi.org/10.1016/j.jvolgeores.2016.06.016

Roecker, S., Ebinger, C., Tiberi, C., Mulibo, G., Ferdinand-Wambura, R., Mtelela, K., . . . Peyrat, S. (2017). Subsurface images of the Eastern Rift, Africa, from the joint inversion of body waves, surface waves and gravity: Investigating the role of fluids in early-stage continental rifting. *Geophysical Journal International*, *210*, 931–950. https://doi.org/10.1093/gji/ggx220

Rogie, J. D., Kerrick, D. M., Chiodini, G., & Frondini, F. (2000). Flux measurements of nonvolcanic CO_2 emission from some vents in Central Italy. *Journal of Geophysical Research*, *105*(B4), 8435–8445. https://doi.org/10.1029/1999JB900430

Rooney, T. O., Bastow, I. D., & Keir, D. (2011). Insights into extensional processes during magma assisted rifting: Evidence from aligned scoria cones. *Journal of Volcanology and Geothermal Research*, *201*(1–4), 83–96. https://doi.org/10.1016/j.jvolgeores.2010.07.019

Rooney, T. O., Furman, T., Yirgu, G., & Ayalew, D. (2005). Structure of the Ethiopian lithosphere: Xenolith evidence in the Main Ethiopian Rift. *Geochimica et Cosmochimica Acta*, *69*(15), 3889–3910. https://doi.org/10.1016/j.gca.2005.03.043

Rooney, T. O., Nelson, W. R., Ayalew, D., Hanan, B., Yirgu, G., & Kappelman, J. (2017). Melting the lithosphere: Metasomes as a source for mantle-derived magmas. *Earth and Planetary Science Letters*, *461*, 105–118. https://doi.org/10.1016/j.epsl.2016.12.010

Rooney, T. O., Nelson, W. R., Dosso, L., Furman, T., & Hanan, B. (2014). The role of continental lithosphere metasomes in the production of HIMU-like magmatism on the northeast African and Arabian plates. *Geology*, *42*(5), 419–422. https://doi.org/10.1130/G35216.1

Saal, A. E., Hauri, E. H., Langmuir, C. H., & Perfit, M. R. (2002). Vapour undersaturation in primitive mid-ocean-ridge basalt and the volatile content of Earth's upper mantle. *Nature*, *419*(6906), 451–455. https://doi.org/10.1038/nature01073

Samrock, F., Kuvshinov, A., Bakker, J., Jackson, A., & Fisseha, S. (2015). 3-D analysis and interpretation of magnetotelluric data from the Aluto-Langano geothermal field, Ethiopia. *Geophysical Journal International*, *202*(3), 1923–1948. https://doi.org/10.1093/gji/ggv270

Sano, Y., & Marty, B. (1995). Origin of carbon in fumarolic gas from island arcs. *Chemical Geology*, *119*(1), 265–274. https://doi.org/10.1016/0009-2541(94)00097-R

Saria, E., Calais, E., Stamps, D. S., Delvaux, D., & Hartnady, C. J. H. (2014). Present-day kinematics of the East African Rift. *Journal of Geophysical Research: Solid Earth*, *119*, 3584–3600. https://doi.org/10.1002/2013JB010901

Self, S., Widdowson, M., Thordarson, T., & Jay, A. E. (2006). Volatile fluxes during flood basalt eruptions and potential effects on the global environment: A Deccan perspective. *Earth and Planetary Science Letters*, *248*(1–2), 517–531. https://doi.org/10.1016/j.epsl.2006.05.041

Seward, T. M., & Kerrick, D. M. (1996). Hydrothermal CO_2 emission from the Taupo Volcanic Zone, New Zealand. *Earth and Planetary Science Letters*, *139*(1–2), 105–113. https://doi.org/10.1016/0012-821X(96)00011-8

Sibson, R. H. (2000). Fluid involvement in normal faulting. *Journal of Geodynamics*, *29*, 469–499. https://doi.org/10.1016/S0264-3707(99)00042-3

Smets, B., Tedesco, D., Kervyn, F., Kies, A., Vaselli, O., & Yalire, M. M. (2010). Dry gas vents ("mazuku") in Goma region (North-Kivu, Democratic Republic of Congo): Formation and risk assessment. *Journal of African Earth Sciences*, *58*(5), 787–798. https://doi.org/10.1016/j.jafrearsci.2010.04.008

Sorey, M. L., Evans, W. C., Kennedy, B. M., Farrar, C. D., & Hausback, B. (1998). Carbon dioxide and helium emissions from a reservoir of magmatic gas beneath Mammoth Mountain, California. *Journal of Geophysical Research*, *103*, 303–323.

Stadler, S., Adem, K., & Gloaguen, R. (2007). *Isotopes as a marker for potential impact of rift tectonics on the groundwater system of the Awash Basin in the East African Rift*. Paper presented at the Proceedings of the 7th International Symposium on Applied Isotope Geochemistry, Stellenbosch, Cape Town, South Africa, September 10–14.

Teclu, A. (2002). *Geochemistry of Dofan-Fentale geothermal prospect* (internal report, 31 pp.). Addis Ababa, Ethiopia: Geological Survey of Ethiopia.

Thrall, R. (1973). Gedemsa Caldera, Ethiopia. *Center for Astrophysics, Dartmouth College, USA, Reprint Series*, *280*, 71–80.

Trestrail, K. R., Rooney, T. O., Girard, G., Svoboda, C., Yirgu, G., Ayalew, D., & Keppelman, J. (2017). Sub-continental lithospheric mantle deformation in the Yerer-Tullu Wellel Volcanotectonic Lineament: A study of peridotite xenoliths. *Chemical Geology*, *455*, 249–263. https://doi.org/10.1016/j.chemgeo.2016.10.013

United Nations Development Programme (UNDP). (1973). Geology, geochemistry and hydrology of hot springs of the East African Rift system within Ethiopia. In *Investigation of geothermal resources for power development* (Tech. Rep. DP/SF/UN 116, 275 pp.). New York, NY: United Nations.

Werner, C., & Brantley, S. (2003). CO_2 emissions from the Yellowstone volcanic system. *Geochemistry, Geophysics, Geosystems*, *4*(7), 1061. https://doi.org/10.1029/2002GC000473

Wignall, P. B. (2001). Large igneous provinces and mass extinctions. *Earth-Science Reviews*, *53*(1–2), 1–33. https://doi.org/10.1016/S0012-8252(00)00037-4

Wilks, M., Kendall, J.-M., Nowacki, A., Biggs, J., Wookey, J., Birhanu, Y., . . . Lewi, E. (2017). Seismicity associated with magmatism, faulting and geothermal circulation at Aluto Volcano, Main Ethiopian Rift. *Journal of Volcanology and Geothermal Research*, *340*, 52–67. https://doi.org/10.1016/j.jvolgeores.2017.04.003.

Williams, F. M., Williams, M. A. J., & Aumento, F. (2004). Tensional fissures and crustal extension rates in the northern part of the Main Ethiopian Rift. *Journal of African Earth Sciences*, *38*(2), 183–197. https://doi.org/10.1016/j.jafrearsci.2003.10.007

WoldeGabriel, G., Aronson, J. L., & Walter, R. C. (1990). Geology, geochronology, and rift basin development in the central sector of the Main Ethiopia Rift. *Geological Society of America Bulletin*, *102*(4), 439–485. https://doi.org/10.1130/0016-7606(1990)102<0439:GGARBD>2.3.CO;2

Wright, T. J., Ebinger, C., Biggs, J., Ayele, A., Yirgu, G., Keir, D., & Stork, A. (2006). Magma-maintained rift segmentation at continental rupture in the 2005 Afar dyking episode. *Nature*, *442*(7100), 291–294. https://doi.org/10.1038/nature04978